ARCHIVES OF ACOUSTICS
2, 1, 3-20 (1977)

APPLICATION OF ULTRASONIC PHYSICS IN MATERIAL TECHNOLOGY*

IGNACY MALECKI

Institute of Fundamental Technological Research (Warszawa)

Measurements of the velocity and attenuation of ultrasonic wave as the basis of the inspection of technological processes. Ultrasonic defectoscopy as used for the detection of internal defects and measurement errors. Correlation between indications of a defectoscope and the mechanical strength of the construction. Determination of elasticity constants of materials. The effect of material grain size upon the attenuation of ultrasonic waves. Stress action vs. increased attenuation. Continuous inspection of the processes: burning of ceramics, polimerization, metal solidification. The effect of microstructure upon the propagation of ultrasonic waves. Properties of materials at low temperatures.

1. Physical foundations of ultrasonic measurement

The main advantage of ultrasonic methods consists in the fact that by means of relatively simple measurements of a few acoustic quantities we can obtain comprehensive information on the structure and properties of materials.

In principle we are dealing with two measurements:

1. measurement of the time-lag Δt between two signals,

2. measurements of difference Δi in the intensity levels of these signals (in decibels).

When a continuous monochromatic signal is used for making the measurements, the equivalent of measuring the time-lag is the measurement of phase differences; a gradual decrease in the amplitude of the signal (in time or in space) corresponds to a difference in intensity. These measurements are made, as a rule, for a certain frequency band and the characteristics $\Delta t(f)$ and $\Delta i(f)$ are thus obtained.

These two basic measurements permit the determination of a number of the acoustic properties of materials, or of the parameters of the object under investigation.

(a) If the distance travelled by a wave between the point from which it is sent and the point at which it is received is Δl, the measurement Δt determines the velocity of propagation of the wave in a given medium:

$$c = \frac{\Delta l}{\Delta t}. \tag{1.1}$$

* Report presented of the Conference «Physics in Industry» Dublin, March 1976.

(b) If the velocity of propagation of the wave is known, the measurement of the time-lag determines the distance, e.g. the distance between the surface of a given object and its internal flaw:

$$\Delta l = c\Delta t. \tag{1.2}$$

(c) The difference Δi in the intensity levels between two points divided by the distance Δl determines the attenuation coefficient a of a given material:

$$a = 0.1151 \frac{\Delta i}{\Delta l} \quad \left[\frac{\text{dB}}{\text{cm}}\right]. \tag{1.3}$$

(d) The differences in the intensity level of waves reflected from the internal heterogenity of a given material is a function of the magnitude and kind of heterogenity.

(e) The maximum of the characteristic $a(f)$ determines the time constant of the acoustic relaxation of the material:

$$\tau = \frac{1}{2\pi f}. \tag{1.4}$$

(f) The pattern of the functions $c(f)$ or $a(f)$ enables us to draw conclusions concerning the mechanism of molecular and atomic losses and of the dynamic quantities of the elasticity constants.

Quantities Δt and Δi may change over time in the technological process, e.g. in the polymerization of plastics. Observation of these changes provides information on the course of this process.

The most interesting measurements from the point of view of learning about the structure of the material are those of Δl and Δi as functions of temperature, especially at low temperatures close to the superconductivity state.

These dependencies concern the kind of material which can be treated as a continuous medium. At very high frequencies (hypersound), when the length of the acoustic wave becomes commensurable with the free path of the phonon, i.e. with the distance between the nodes of the crystal lattice, a classical approach does not suffice. It is necessary then to resort to the presentation of the acoustic wave as a stream of phonons, i.e. to take into consideration the quantum nature of the phenomena which occur. The methods of measurement change correspondingly; for instance the tunnel effect is used for generation, and opto-acoustic methods are frequently used in reception.

Ultrasonic methods are, in many cases, used in parallel with other methods (e.g. X-rays) for determining the same properties of the materials.

The following considerations are decisive in the choice of the ultrasonic method:

1. the properties of the material — the majority of constructional materials are «transparent» for ultrasound, while electromagnetic waves and streams of elementary particles are reflected almost completely;

2. the ultrasonic equipment is relatively inexpensive and simple in use;

3. the passage of an ultrasonic wave does not, in most cases, produce additional effects similar to those which accompany, for example, the propagation of X-rays.

We shall now review the applications of ultrasonic methods in material engineering, with special emphasis on those problems in which close cooperation between the technologist and the physicist is needed.

2. Detection of internal flaws in materials and geometric measurements

The detection of flaws in materials is the oldest technological application of ultrasound. The first ultrasound flaw detectors (FIŘESTONĚ, SOKOLOV) date back to the 1930's. Even at the first International Conference of Non-Destructive Testing (Brussels 1955) [1] it was shown that ultrasonic methods provide an important tool for technological control in industry. Since that time the importance of these methods has been increasing steadily; it is estimated that at present about 30% of industrial control equipment based on non-destructive methods use ultrasonic techniques.

The most common equipment operates by measuring the delay time and the intensity of an impulse reflected from a flaw. A modern flaw detector has extensive electronics, providing a high degree of automation of measurement. In addition to universal devices a number of specialized devices have been built, e.g. a device serving for detecting internal flaws in rails. There is a whole group of instruments for measuring (usually by resonance methods) the thickness of walls accessible from one side only, as for example in high pressure containers. Actually an ultrasonic control system for testing motor vehicle tyres is progressing; by means of probe-heads switching the high precision and high speed is achieved in testing.

In spite of tremendous progress in flaw detector design, the process of improving them has not yet been completed. This applies both to electronic and to acoustical parts of equipment. Figure 1a shows a typical transmission system and Fig. 1b — a receiving system for equipment measuring the speed and attenuation of ultrasonic waves. From the research point of view the most interesting problem is that of establishing a correlation between flaw signal in the equipment and the mechanical weakening of the material by a flaw. As we have already mentioned, the method used most frequently compares results of the tested object with those from a sample with a standard flaw. There are, of course, also more general studies of a scientific nature [2, 3]. The problem here is to solve complex diffraction problems. Let us recall that the theory of ultrasonic wave reflection from an obstacle in a solid was solved only 20 years ago and only for the simplest case [4]. In periodicals dealing with acoustics quite a number of articles dealing with this problem may still be encountered. The complication is that both the transducer and the obstacle generate waves of different types, causing complex secondary reflections [5].

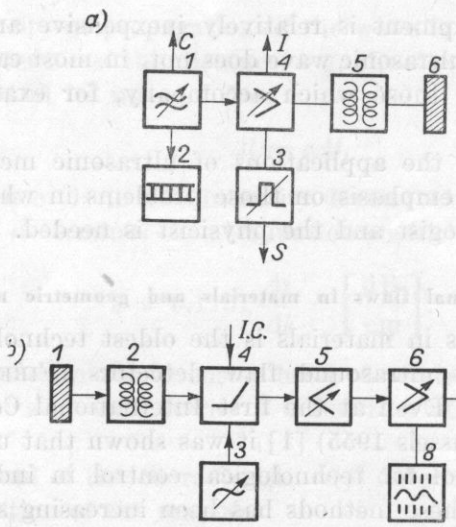

Fig. 1. The electronic system of the equipment for measuring velocity and attenuation
a) Transmitting part. *1* – oscillator, *2* – frequency meter, *3* – pulse generator, *4* – amplifier, *5* – matching circuit, *6* – transmission head.
b) Receiving part. *1* – receiving head, *2* – matching circuit, *3* – oscillator, *4* – frequency converter, *5* – attenuator, *6* – amplifier, *7* – oscilloscope, *8* – information processing.
C – continuous wave, *I* – pulse, *S* – synchronizing pulse

The second part of the problem is an evaluation of the extent to which a single flaw or a set of flaws detected by a flaw detector results in a lowering of the mechanical strength of an object. Extensive experimental work is being carried on in order to determine this relationship for various types of flaws [6].

On this basis standards have been elaborated [7]; in testing welded joints, for example, five classes of flaws have been established and the quality of the joint is determined according to them. This work is conducted by the International Institute of Welding [8]. The best practical results are given by the comparative method, using as a standard an element with artificial flaws [9] (Fig. 2).

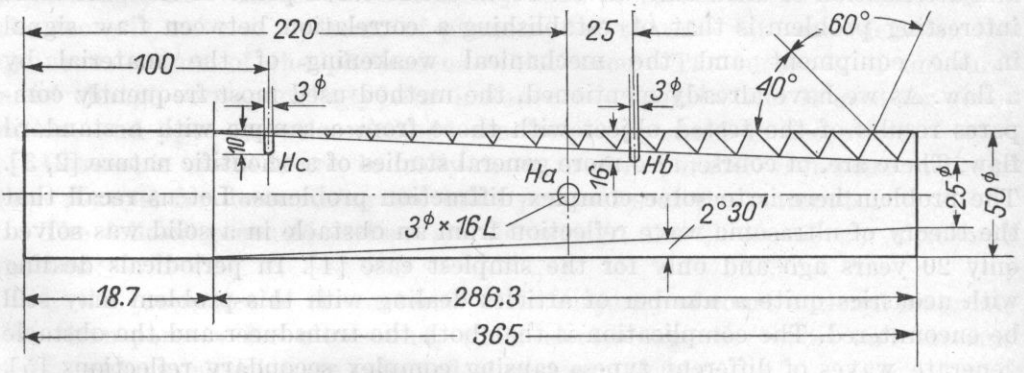

Fig. 2. Standard element for surface waves

3. Determination of the elastic constants

In a homogeneous medium there is a simple relationship between the velocity of acoustic wave propagation and the elastic constants. For the VOIGT model we have

$$\frac{1}{2}\varrho c_T^2 = \frac{\left[\frac{E}{2(1+\nu)}\right]^2 + \omega^2\eta^2}{\frac{E}{2(1+\nu)} + \sqrt{\left[\frac{E}{2(1+\nu)}\right]^2 + \omega^2\eta^2}}, \tag{3.1}$$

$$\frac{1}{2}\varrho c_L^2 = \frac{\left[\frac{(1-\nu)E}{(1+\nu)(1-2\nu)}\right]^2 + \omega^2\eta^2}{\frac{(1-\nu)E}{(1+\nu)(1-2\nu)} + \sqrt{\left[\frac{E(1-\nu)}{(1+\nu)(1-2\nu)}\right]^2 + \omega^2\eta^2}}, \tag{3.2}$$

where ϱ is the density of the material, c_T, c_L – the velocities of tranverse and longitudinal waves, E, η – elasticity and viscosity elements in the Voigt model, ν – Poisson's ratio.

On the basis of the measurement of the dynamic elastic coefficient, the specific heat at constant volume is determined. It turns out that the materials of the concrete type, i.e. materials [10] with distinct heterogeneity in the macrostructure, display a distinct velocity dispersion (Fig. 3). It should be surmised that the elastic modulus E increases (Fig. 4) and the viscosity decreases (Fig. 5) with frequency.

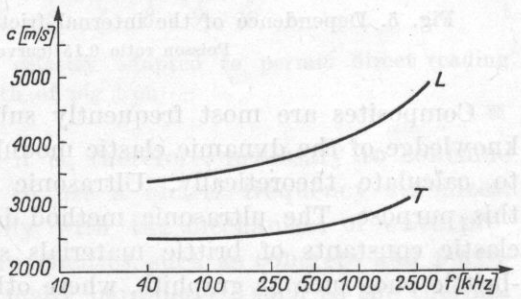

Fig. 3. Wave dispersion in concrete (slab 40×40×5 cm) (Drescher)
L – longitudinal wave, T – transversal wave

In recent years composites have been more and more frequently used; they are, as we know, ceramics, metallic materials or polymers strengthened with fibres or whiskers. It has turned out that ultrasonic methods are very useful for testing the elastic properties of these new materials. Generally speaking, the elasticity modulus E_k of the composite is less than the weighted sum of the moduli of the components:

$$E_k < E_a V_a + E_b V_b \tag{3.3}$$

(V_a, V_b are volume proportions).

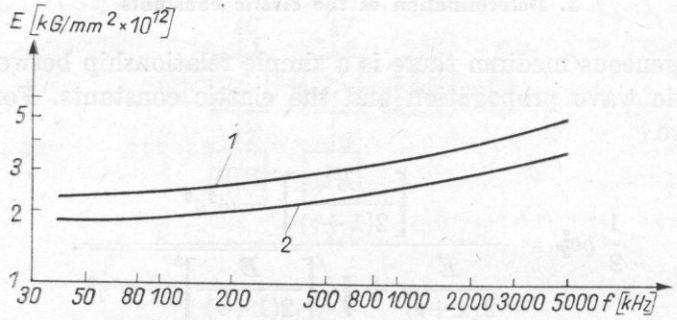

Fig. 4. Dependence of the modulus of elasticity E on frequency
Poisson ratio 0.15 (curve *1*) and 0.30 (curve *2*)

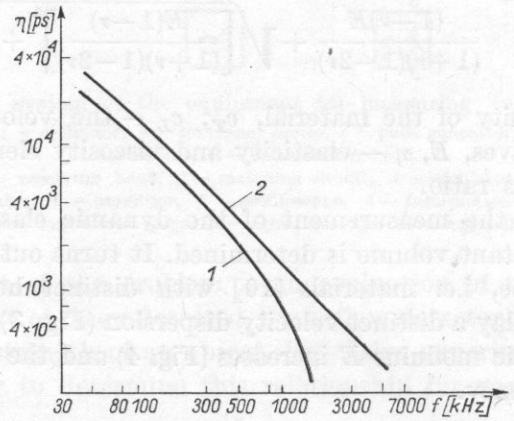

Fig. 5. Dependence of the internal friction coefficient on frequency (Drescher)
Poisson ratio 0.15 (curve *1*) and 0.30 (curve *2*)

Composites are most frequently subjected to dynamic stresses and thus knowledge of the dynamic elastic moduli is necessary. It is difficult, however, to calculate theoretically. Ultrasonic measurements are indispensable for this purpose. The ultrasonic method is especially useful for measuring the elastic constants of brittle materials such as ceramic materials, and semi-brittle ones such as graphite, where other methods produce no results. Resonance methods at frequencies up to 100 kHz, and pulse methods at frequencies between 1 and 100 MHz, are used for these measurements.

4. Testing the mechanical strength

The magnitude of the elastic constants is related directly to the strength of the materials. Research has shown that for some groups of brittle materials (concrete, cast iron) there is a relationship between the velocity of propagation of the ultrasonic waves and the mechanical strength R_c (Fig. 6). This

makes possible an extensive application of ultrasonic methods for controlling building constructions, especially bridge constructions. Special flaw detectors are used for measuring the strength of cast iron using scales on which both the velocity of the ultrasonic waves and the strength of the material can be immediately read [12] (Fig. 7). The velocity measurement must be very precise

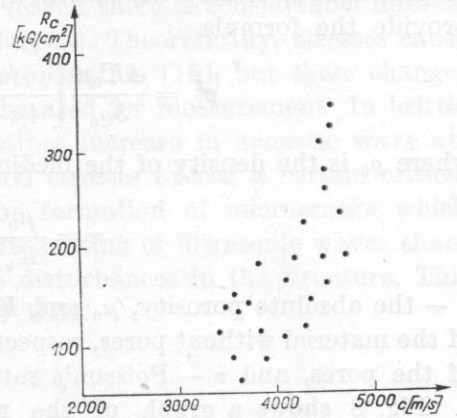

Fig. 6. Dependence of mechanical strength on wave velocity for concrete (experimental data) (Pawłowski)

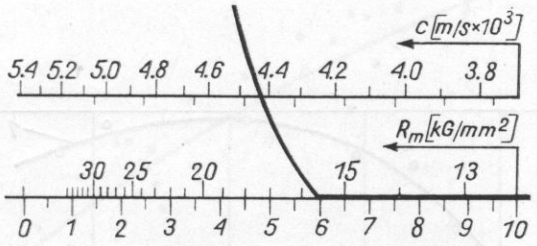

Fig. 7. The meter scale for ultrasonic wave velocity adapted to permit direct reading of the strength of pig iron

(the error must not exceed 0.2 %) and it is, therefore, necessary to continue improving the electronic systems and to use a quartz frequency stabilizer. Scientific studies are concerned primarily with the mechanism of wave propagation in media with stochastic heterogeneities, such as concrete and polycrystals. This mechanism depends upon many parameters, such as the thermal conductivity at the boundaries of the heterogeneities, their elastic anisotropy, and the ratio of their dimensions to the wavelength. A fairly good approximation is obtained by the formula for the attenuation coefficient [13],

$$\alpha = 4\left(\frac{\overline{\Delta c}}{c}\right)^2 k^4 D^3 \quad \text{for } kD \ll 1, \tag{4.1}$$

$$\alpha = \frac{\sqrt{\pi}}{2}\left(\frac{\overline{\Delta c}}{c}\right)^2 k^2 D \quad \text{for } kD \gg 1, \tag{4.2}$$

where D is average diameter of a heterogenity, k is the wave number and $\Delta c/c$ — relative change of the wave velocity due to the inhomogeneities in the medium.

The propagation of ultrasonic waves may then provide some idea of the nature of heterogeneity.

Experience shows that the velocity of wave propagation in such materials as porcelain is clearly dependent upon porosity. Theoretical calculations [14] provide the formula

$$c_L^2 = \frac{4K_0\mu}{3\varrho_0}\left[\frac{3}{4\mu+3\varepsilon(1+\varkappa)\sigma^2}+\frac{1-\varkappa\varepsilon}{1-\varepsilon}\right], \tag{4.3}$$

where ϱ_0 is the density of the medium without pores,

$$\varkappa = \frac{\mu_0}{K_0}-\frac{3}{2}\frac{(1-\nu)}{(1+\nu)}, \tag{4.4}$$

ε — the absolute porosity, μ_0 and K_0 — the shear modulus and bulk modulus of the material without pores, respectively, σ^2 — the standard volume deviation of the pores, and ν — Poisson's ratio.

Fig. 8 shows a graph of the relationship $c_L(\varepsilon)$ versus temperature of burning. Measurements confirm theoretical expectations.

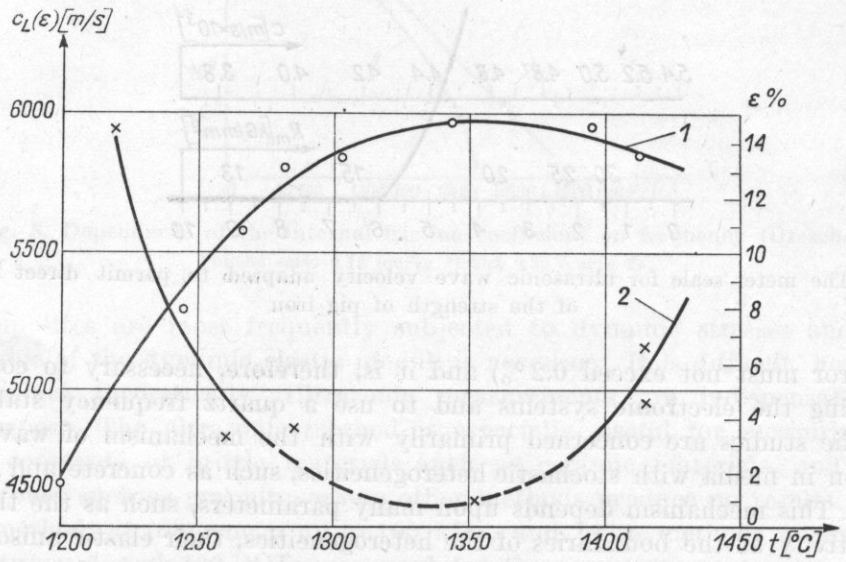

Fig. 8. Relation between wave velocity c (curve *1*) and porosity ε (curve *2*) for technical porcelain (Ranachowski)

The mechanical strength of porcelain depends, of course, upon its porosity. The ultrasonic method is the only one which can be used for testing the mechanical strength of large insulators in which pores are sometimes not uniformly distributed and which thus may be subject to the danger of local cracks.

5. Testing the stress of materials

The knowledge of the spatial distribution of stresses in mechanical elements is of great importance for the construction and operation of machines. Tensometric methods may only be used for the testing of surface stresses, while elastooptic methods require the construction of models not fully commensurable with the original machine. For this reason there is considerable interest in the use of ultrasonic methods for this purpose. Theoretically, stresses cause changes in the velocity of acoustic wave propagation [15], but these changes are so small that in practice they cannot be used for measurement. In brittle and semi-brittle materials, however, a distinct increase in acoustic wave attenuation occurs in areas where the internal stresses exceed a certain critical value. This phenomenon is caused by the formation of microcracks which disperse the wave. Fig. 9 shows how the attenuation of ultrasonic waves changes as a function of the percentage of the disturbances in the structure. This applies to testing frequencies from 0 to 30 MHz.

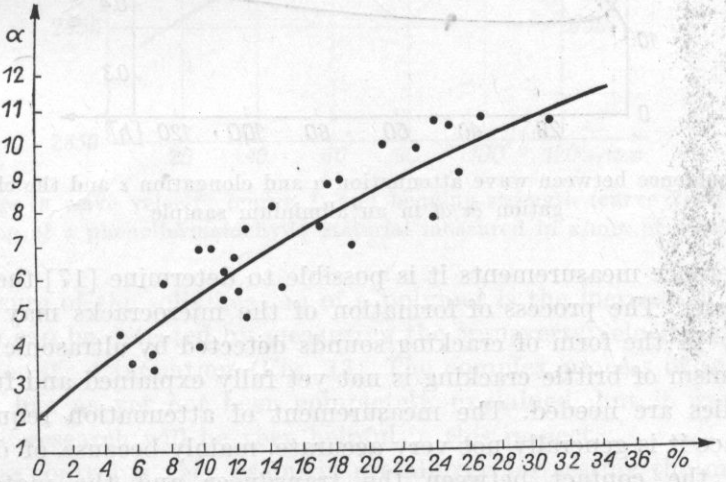

Fig. 9. Wave attenuation as a function of the percentage of area of the disturbed structure of a ceramic insulator

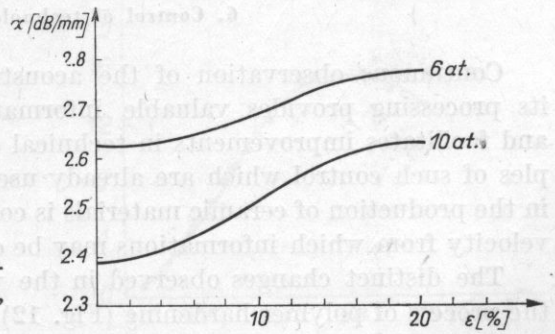

Fig. 10. Attenuation α of the wave in polypropylene in the elongation function ε, with different injection pressures

Changes in the attenuation of a 2.5 MHz ultrasonic wave can be clearly observed (Fig. 10) during the stretching of a polymer (polypropylene) sample. This is caused by reorientation of the macromolecules due to stretching. The creep effect in metals also produces changes in attenuation (Fig 11) and thus opens the possibility of determining the limits of elasticity and plasticity [16].

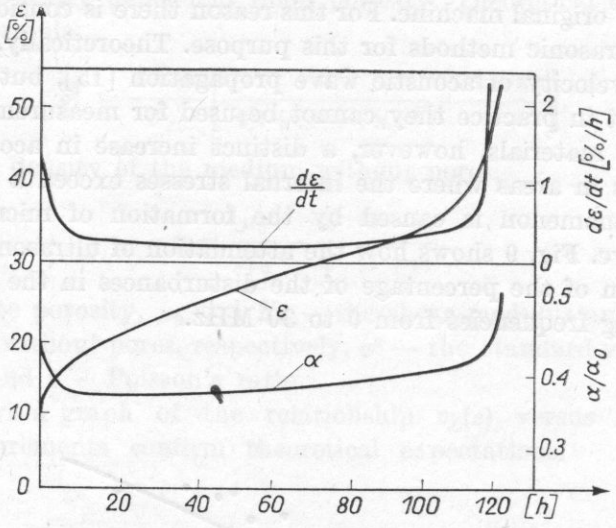

Fig. 11. Dependence between wave attenuation α and elongation ε and the change in elongation $\partial\varepsilon/\partial t$ in an aliminium sample

By difference measurements it is possible to determine [17] the anisotropy of the stresses. The process of formation of the microcracks may be monitored directly in the form of cracking sounds detected by ultrasonic sensor [18]. The mechanism of brittle cracking is not yet fully explained and further theoretical studies are needed. The measurement of attenuation requires improvement, since it is generally not very accurate, mainly because of disturbances caused by the contact between the transducer and the material. Pulse methods or resonance ones are used depending upon the parameters.

6. Control of technological processes

Continuous observation of the acoustic parameters of a material during its processing provides valuable information on the course of this process and facilitates improvements in technical control. We shall give several examples of such control which are already used in practice. The reheating process in the production of ceramic materials is controlled by measurement of the wave velocity from which informations may be obtained concerning pores formation.

The distinct changes observed in the velocity of wave propagation during the process of polymer hardening (Fig. 12) may be used as a test of the pattern

of the process. The changes in wave velocity are caused by the reorientation θ of polymer molecules in accordance with the relationship

$$\theta = \frac{1-(c_n/c)^2}{1-(c_n/c_0)^2}, \tag{6.1}$$

where c_n is the wave velocity in a non-orientated amorphous polymer, c_0 — the wave velocity in an ideally orientated polymer, and c — the actual wave velocity.

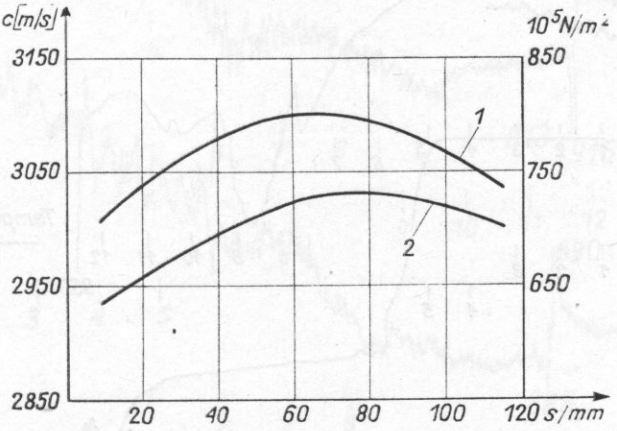

Fig. 12. Change in wave velocity (curve *1*) and bending strength (curve *2*) in the process of hardening of a phenolformaldehyde material measured in s/mm of pressing time

The measure of the solidification of a polymer is the increase in shear elasticity, which can be detected by measuring the transverse velocity of the ultrasonic wave or its attenuation (Fig. 13). The complex process of solidification of polymers has as yet not been completely explained, but it would appear that acoustic research will be very helpful in this respect.

Ultrasonic control is very useful in metallurgy for testing the melting process and phase changes. Both occur at virtually constant temperature, but

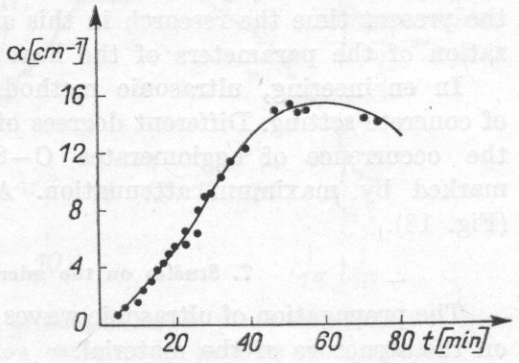

Fig. 13. Attenuation as a function of polymerization time for a polyester (f = 3 MHz) (Kunnert)

the ultrasonic attenuation is considerably increased during melting (Fig. 14). In phase transformations the temperature hysteresis takes place and sudden changes in attenuation can be observed, as in Fig. 15, which pertains to pure iron. In Fig. 16 we have an analogous graph for low carbon (0.1 %) Armco steel. Probably, because of the influence of the impurities, the transformation in this material takes place gradually with declining temperature. Another example is the influence of temperature on wave attenuation (Fig. 17).

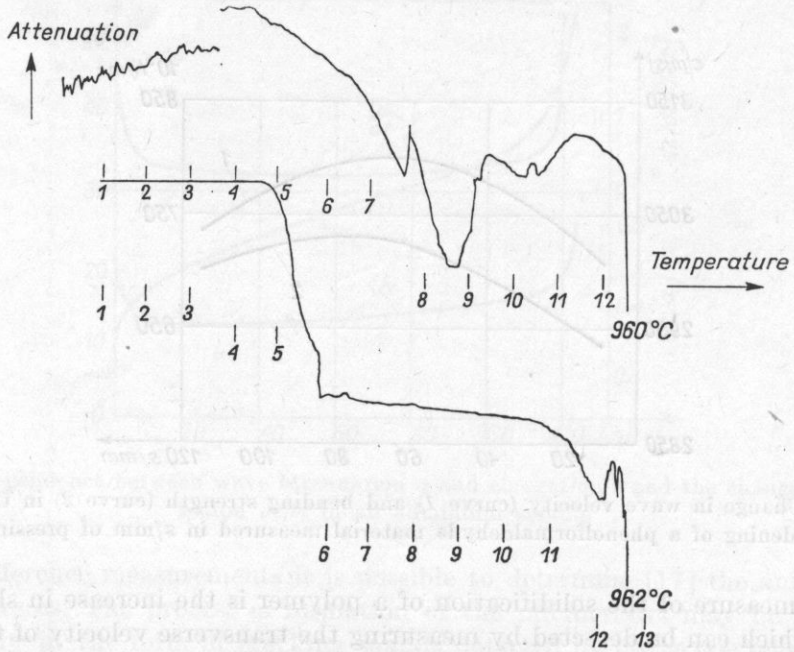

Fig. 14. Changes in wave attenuation as a function of temperature in melting and solidifying pure silver (Kiedrzyński)

In view of the small number of research papers on the influence of the melting or of the solidification of metals on acoustic wave propagation, generalizations concerning these relationships are still lacking. Nevertheless, at the present time the research in this area may be very helpful in the optimization of the parameters of the heat treatment process.

In engineering, ultrasonic methods are used for studying early stages of concrete setting. Different degrees of hydration may be distinguished, while the occurrence of agglomerates C—S—H ($CaSiO_2$) and C—H($CaOH_2$) is marked by maximum attenuation. Audible frequencies are also used here (Fig. 18).

7. Studies on the microstructure of materials

The propagation of ultrasonic waves produces direct or indirect information on the structure of the material.

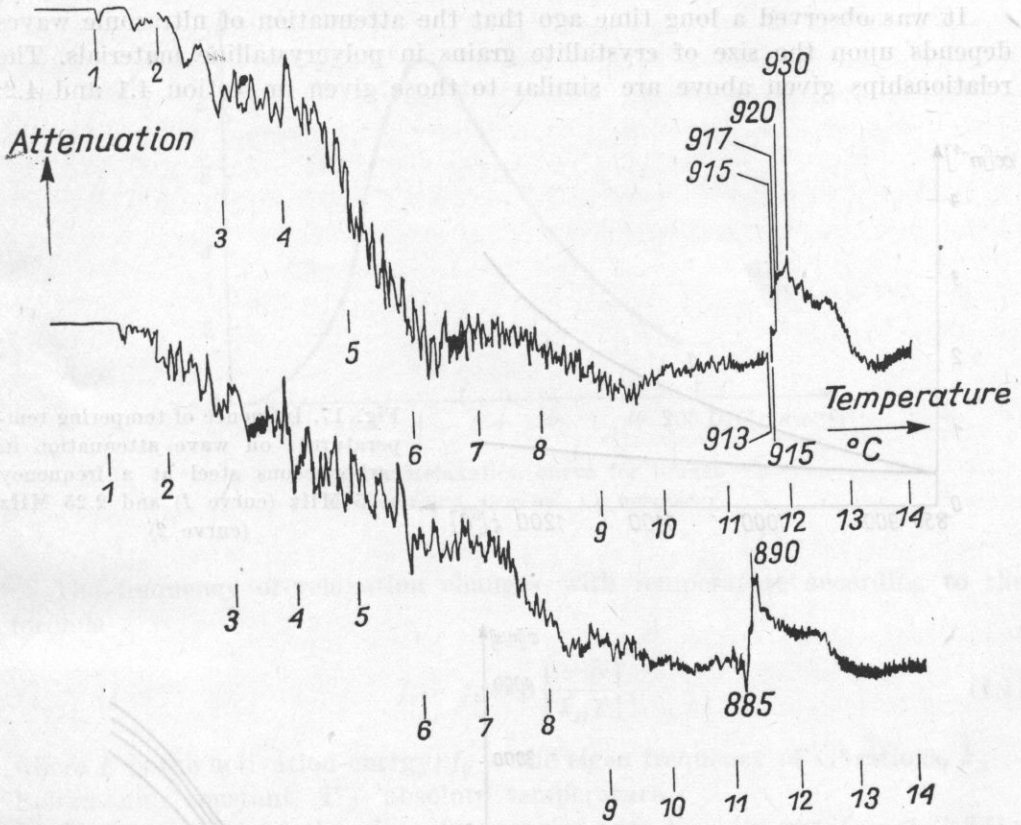

Fig. 15. Changes in attenuation as a function of temperature in phase transformation from alpha to gamma and vice versa for pure iron (Kiedrzyński)

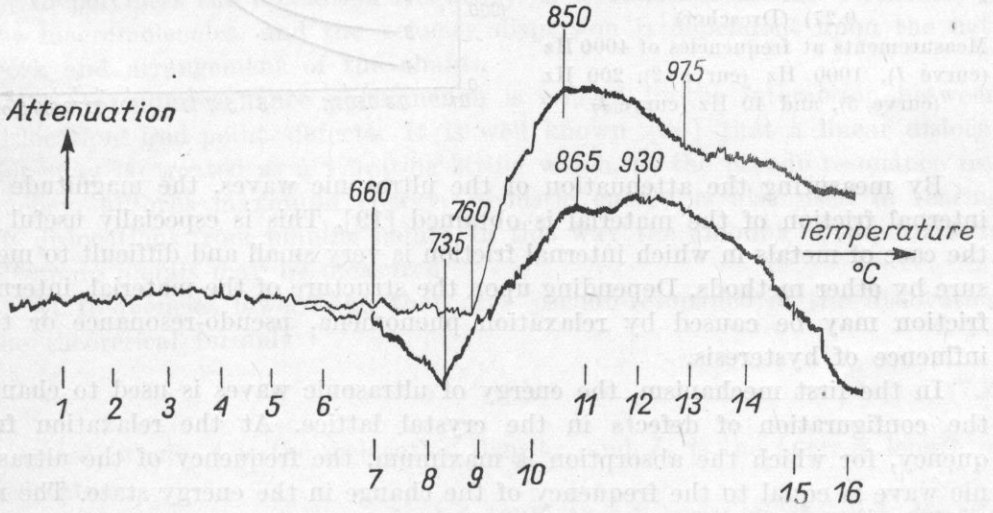

Fig. 16. Changes in attenuation as a function of temperature in phase transformation from alpha to gamma and vice versa for low carbon steel (Armco) (Kiedrzyński)

It was observed a long time ago that the attenuation of ultrasonic waves depends upon the size of crystallite grains in polycrystalline materials. The relationships given above are similar to those given in section 4.1 and 4.2.

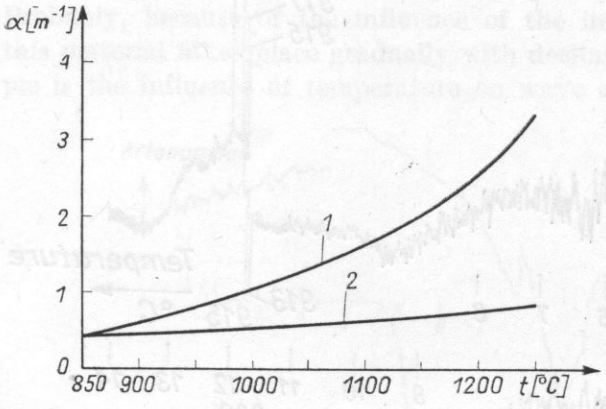

Fig. 17. Influence of tempering temperature t on wave attenuation in carbonaceous steel at a frequency of 5 MHz (curve *1*) and 2.25 MHz (curve *2*)

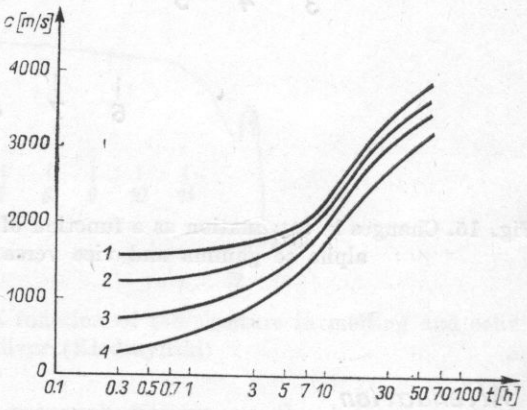

Fig. 18. Changes in longitudinal wave velocity in the cement paste setting process (at a water to cement ratio of 0.27) (Drescher)
Measurements at frequencies of 4000 Hz (curve *1*), 1000 Hz (curve *2*), 200 Hz (curve *3*), and 40 Hz (curve *4*)

By measuring the attenuation of the ultrasonic waves, the magnitude of internal friction of the material is obtained [19]. This is especially useful in the case of metals in which internal friction is very small and difficult to measure by other methods. Depending upon the structure of the material, internal friction may be caused by relaxation phenomena, pseudo-resonance or the influence of hysteresis.

In the first mechanism, the energy of ultrasonic waves is used to change the configuration of defects in the crystal lattice. At the relaxation frequency, for which the absorption is maximum, the frequency of the ultrasonic wave is equal to the frequency of the change in the energy state. The relaxation curve for bronze is given as an example on Fig. 19. On this basis we can find the magnitude of the activation energy.

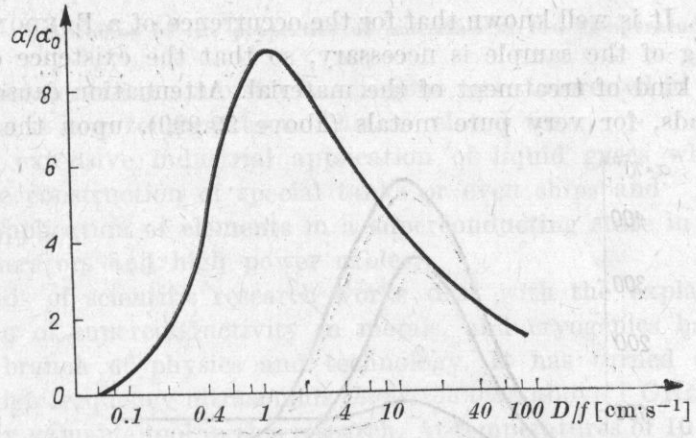

Fig. 19. Relaxation curve for bronze
D – crystallite diameter, f – frequency

The frequency of relaxation changes with temperature according to the formula

$$f_r = f_0 \exp\left\{\frac{-E}{k_B T}\right\}, \tag{7.1}$$

where E is the activation energy, f_0 – the eigen frequency of vibrations, k_B – Boltzmann's constant, T – absolute temperature.

Typical values of the eigen frequencies are: for nitrogen $f_0 = 4.35$ THz, for carbon $f_0 = 2.5$ THz.

In polymers the relaxation frequency is a function of the structure of the macromolecules, and the velocity dispersion is dependent upon the network and arrangement of the chains.

The pseudo-resonance phenomenon is related to the interaction between dislocations and point defects. It is well known [20] that a linear dislocation may be treated as a vibrating string which, at the pseudo-resonance frequency, absorbs maximum energy. Acoustic energy is also used in tearing off dislocations from pinning points. In this way the amount of impurities in ultrapure metals may be measured.

At frequencies lower than that of a pseudo-resonance of the dislocation the theoretical formula

$$a = \Lambda L_0^4 \omega^2 \tag{7.2}$$

is tested, where Λ is the dislocation density, and L_0 is the average length of dislocation.

At temperatures of the order of 100K the dislocations interact directly with the crystal lattice; this is related to the appearance of BORDONI peaks

[21] (Fig. 20). It is well known that for the occurrence of a BORDONI peak previous crushing of the sample is necessary, so that the existence of the peak indicates the kind of treatment of the material. Attenuation caused by dislocations depends, for very pure metals (above 99.999), upon the percentage

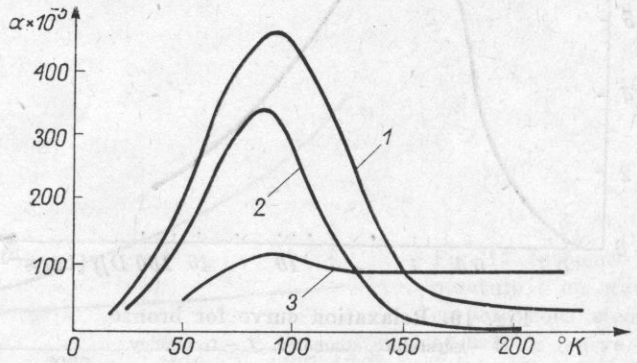

Fig. 20. Wave attenuation for copper indicating the presence of Bordoni peaks
Curve *1* – unannealed copper, curve, *2* – annealed copper, curve *3* – monocrystal of copper

of impurities (Fig. 21). As the amount of impurities increases, the dislocation loops become shorter, the frequency at which the maximum occurs increases and the maximum itself becomes flattened.

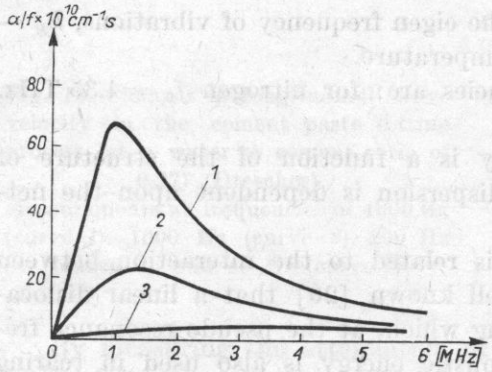

Fig. 21. The dependence of attenuation in very pure aluminum on the impurity density
Curve *1* – 4×10^{-5}% impurities, curve *2* – 19×10^{-5}% impurities, curve *3* – 65×10^{-5}% impurities

Attenuation arising from hysteresis in the material results from the non-linearity of the stress-strain function, which is related to the lowering of strength which, in turn, is related to fatigue processes. The problem is of great practical importance because of the danger of the excessive fatigue of material.

It is worth noting that ultrasound can very well be used not only for measurement, but also for bringing about fatigue in the material. The time of operation for ultrasound is many times shorter than for mechanical fatigue. Especially encouraging results were obtained in the ultrasonic fatigue of hoisting ropes [22]. The frequency of 22 kHz and an electrical power of 600 W applied about 2 minutes are sufficient to obtain visible fatigue in the sample.

8. Studies of the properties of materials at low temperatures

In the last decade the industry has become more interested in the behaviour of materials at low temperatures. This is related to:

1. more extensive industrial application of liquid gases which, in turn, requires the construction of special tanks or even ships and
2. the application of elements in a superconducting state in the construction of generators and high power cables.

Thousands of scientific research works deal with the explanation of the phenomenon of superconductivity in metals, and cryogenics has become an important branch of physics and technology. It has turned out, however, that very high frequency ultrasounds (*hypersounds*), above 1 GHz, may become an especially valuable tool in this research. At temperatures of 10 K the average free path of the phonon is of the order of $10^{-2} \div 10^{-4}$ cm, and so it is of the same order of magnitude as a hypersonic wave length at a frequency of the order of 10 MHz $\div$ 1 GHz.

Under these conditions quantum phenomena are clearly observed and the hypersonic wave must be treated as a flux of phonons. The theory of acoustic phonon collisions [23] with electrons and thermophonons provides an explanation of many phenomena occurring in the state of superconductivity. The observation of the propagation of hypersonic waves gives indirect measurements of the mechanical and electromagnetic parameters of superconductive materials. Studies in this field are at present only in the initial stage, but it should be expected that they will produce valuable results as a result of the common efforts of physicists and technologists.

9. Acknowledgment

Most of the results of experimental work were obtained in the laboratories of the Institute of Fundamental Technological Research in Warsaw, and especially from the departments headed by Professor Z. PAWŁOWSKI and Professor J. RANACHOWSKI.

References

[1] *Proceedings of International Conference on Nondestructive Testing*, Brussels 1956.

[2] L. FILIPCZYŃSKI, *Radiation of acoustic waves for pulse ultrasonic flaw detection purposes*, Proc. 2nd Ultrasonic Conference, PWN, Warszawa 1956.

[3] J. WEHR, *The influence of attenuating screens on the directivity pattern of ultrasonic transducers*, Proc. Vibr. Problems, **2**, 283 (1962).

[4] C. F. YING, R. T. TRUELL, *Scattering of a plane longitudinal wave by a spherical obstacle in an isotropically elastic solid*, J. Appl. Phys., **27**, 1086 (1956).

[5] M. REDWOOD, *The generation of secondary signals in the propagation of ultrasonic waves*, Proc. Phys. Soc. London, **72**, 841 (1958).

[6] L. FILIPCZYŃSKI, Z. PAWŁOWSKI, J. WEHR, *Ultrasonic methods of testing materials*, Butterworths, London 1966.

[7] J. and H. KRÄUTKRÄMER, *Ultrasonic testing of materials*, Springer, Berlin 1969.

[8] Z. PAWŁOWSKI, *Problems of ultrasonic testing in welding*, XXI Annual Assembly of International Institute of Welding, Warsaw 1968.

[9] N. SINCLAIR, *Consideration of establishing ultrasonic test acceptance standards*, Materials Evaluation, **25**, 118 (1967).

[10] E. DRESCHER, *New developments in non-destructive testing of non-metalic materials*, Rilem 3rd Symposium, Constantá 1974.

[11] I. K. MACKENZIE, *The elastic constants of a solid containing spherical holes*, Proc. Phys. Soc., London, **63**, 2 (1950).

[12] Z. PAWŁOWSKI, *Experience in the evaluation of grey cast iron tensile strength with ultrasonics*, 7th Int. Conf. on Nondestructive Testing, Warsaw 1973, Paper J-07.

[13] W. ROTH, *Scattering of ultrasonic radiation in polycrystalline metals*, J. Appl. Phys., **19**, 901 (1948).

[14] J. RANACHOWSKI, *Propagation of ultrasonic waves in porous ceramics*, Ultrasonics, **13**, 203 (1975).

[15] I. MALECKI, *Physical foundations of technical acoustics*, Pergamon Press, Oxford 1968.

[16] T. HIRONE, *Quality inspection of materials*, 3rd International Conference on Nondestructive Testing, Tokyo 1960, p. 317.

[17] L. D. CRECRAFT, *Ultrasonic measurement of stresses*, Ultrasonic, **6**, 117 (1968).

[18] Z. PAWŁOWSKI, R. RUŁKA, *Measurement of stress using the Barkhausen effect*, 7th Int. Conf. on Nondestructive Testing, Warsaw 1973, Paper J-13.

[19] M. ZENER, *Elasticity and anelasticity of metals*, University Press, Chicago 1948.

[20] A. GRANATO, K. LÜCKE, *Theory of mechanical damping due to dislocations*, J. Appl. Physic, **27**, 583, (1959).

[21] P. G. BORDONI, *Elastic and anelastic behaviour of some metals at very low temperatures*, J. Acoust. Soc. America, **26**, 495 (1954).

[22] B. PEŃSKO, O. WISZNIEWSKI, L. FILIPCZYŃSKI, *Application of ultrasound to fatigue testing of steel wires and cables*, Proc. Vibr. Probl., **14**, 285 (1973).

[23] I. MALECKI, *The use of the phonon representation in acoustics*, 6th Conf. on Acoustics, Budapest 1976.

Received on 22nd February 1976

ARCHIVES OF ACOUSTICS
2, 1, 21-23 (1977)

BASIC ACOUSTIC PARAMETERS OF ORGANIC SOLVENTS USED IN ULTRASONIC CLEANING

BOGDAN NIEMCZEWSKI, TERESA SZLAGOWSKA

Tele- and Radio Research Institute (Warszawa)

Sound velocities have been measured and the specific acoustic impedance calculated for the following solvents used in the process of ultrasonic cleaning (commercial technical products): trichloroethylene, tetrachloroethylene, 1,1,1-trichloroethane (Baltane), trichlorotrifluoroethane (Freon TF) and dibromotetrafluoroethane, known as freon 114B2.

The solvents preferred for use in industrial ultrasonic cleaning processes are:

1. trichloroethylene,
2. tetrachloroethylene,
3. 1,1,1-trichloroethane (trade names Chlorothene, Genklene, Baltane),
4. trichlorotrifluoroethane also known under the name of freon 113 (trade names Freon TF, Arklone P, Flugene 113).

When designing cleaning equipment intended for operation with these solvents and when developing technological processes, it is frequently necessary to make calculations involving the velocity of sound propagation, and acoustic impedance of these liquids is needed. Unfortunately, only for the first two of the above-mentioned liquids can these parameters be found in the literature. Furthermore, for tetrachloroethylene various sources cite different values of propagation velocity (e. g. L. BERGMAN — 1066 m/s, while W. SCHAAFF — 1053 m/s).

The present authors have measured the sound velocity c (by means of an interferometer) and the density ϱ (using a Mohr-Westphal hydrostatic balance) at various temperatures for all the above liquids. The coefficients $\Delta c/\Delta T$ and $\Delta \varrho/\Delta T$ and the acoustic impedances ϱc at 20°C were then determined. The liquid density ϱ was measured with an accuracy of 0.001 g/cm^3, and the sound velocity c with an accuracy of 1 m/s. Values corresponding to 20°C were read of the graphs shown in Fig. 1. Freshly distilled technical products were used for the investigations, since with such solvents we are concerned in practice. The solvents used were:

— trichloroethylene from Chemical Plant «Oświęcim» according to PN-69/C-88025,

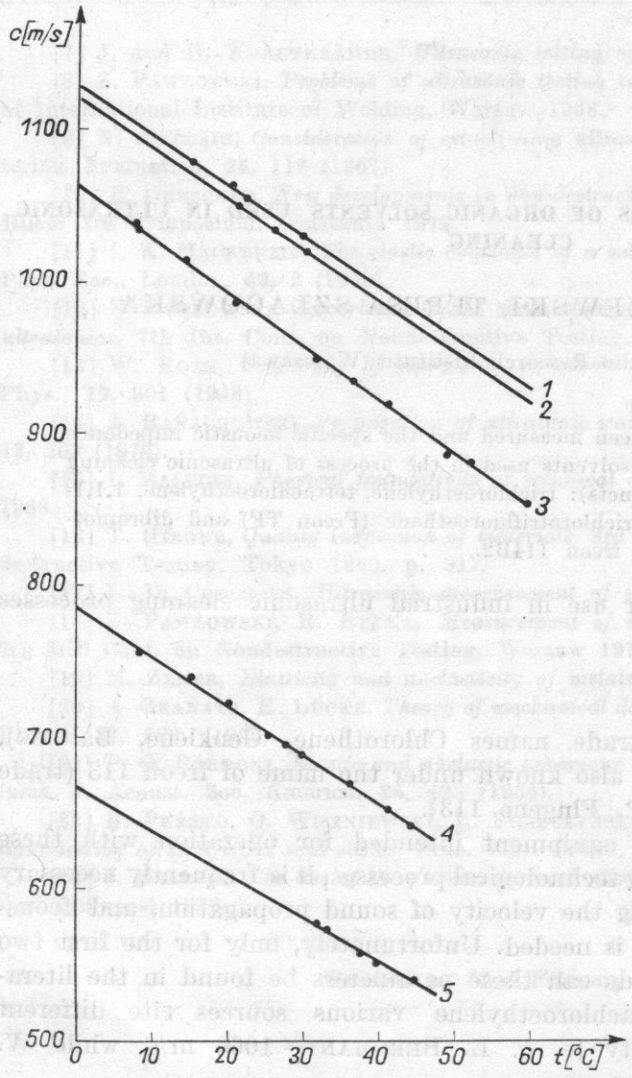

Fig. 1. The dependence of the sound propagation velocity on temperature in the five tested liquids

1 – tetrachloroethylene, *2* – trichloroethylene, *3* – 1,1,1-trichloroethane, *4* – freon 113, *5* – freon 114B2

– tetrachloroethylene from Chemical Plant «Oświęcim» according to PN-70/6026-44,

– 1,1,1-trichloroethane Baltane from Rhone Progil (France),

– trichlorotrifluoroethane Freon TF produced by the concern Du Pont.

Furthermore, the acoustic parameters of dibromotetrafluoroethane (known as freon 114 B2) produced by Nitrogen Plant «Tarnów» were also measured. Its physical properties are similar to those of trichlorotrifluoroethane (but the relevant acoustic data are also not available in the literature).

The results obtained are compared in Table 1.

It is worth pointing out that both the tested freons are remarkable in possessing sound propagation velocities amongst the lowest of the liquids tested

Table 1. Comparison of obtained results

Substance		c at 20°C $\left[\frac{\text{m}}{\text{s}}\right]$	$\Delta c/\Delta T$ $\left[\frac{\text{m}}{\text{s deg}}\right]$	ϱ_4^{20} $\left[\frac{\text{g}}{\text{cm}^3}\right]$	$\Delta\varrho/\Delta T \times 10^{-5}$ $\left[\frac{\text{g}}{\text{cm}^3\,\text{deg}}\right]$	$\varrho c \times 10^3$ at 20°C $\left[\frac{\text{g}}{\text{cm}^2\,\text{s}}\right]$
C_2Cl_4	tetrachloroethylene Cl Cl | | C=C | | Cl Cl	1063	-3.3^{30}_{15}	1.618	-169^{45}_{20}	172.0
C_2HCl_3	trichloroethylene Cl Cl | | C=C | \\ H Cl	1055	-3.5^{30}_{15}	1.464	-173^{50}_{20}	154.4
$C_2H_3Cl_3$	1,1,1-trichloro-ethane H Cl | | H–C–C–Cl | | H Cl	992	-3.56^{60}_{5}	1.333	-172^{50}_{20}	132.2
$C_2Cl_3F_3$	trichlorotrifluoro-ethane Cl Cl | | F–C–C–F | | Cl F	720	-3.23^{45}_{10}	1.576	-222^{30}_{15}	113.5
$C_2F_4Br_2$	dibromotetrafluoro-ethane F F | | Br–C–C–Br | | F F	609*)	-2.9^{45}_{30}	2.181	-319^{35}_{15}	132.8

x) Extrapolated value.

so far. In the table arranged by W. SCHAFFS containing data on 368 organic liquids only 8 have sound velocities smaller than those in freon 113 and only three smaller than in freon 114B2.

Received on 21st January 1976

ARCHIVES OF ACOUSTICS
2, 1, 25-33 (1977)

ACOUSTICAL STUDIES OF THE SOLVATION OF $ZnCL_2$ IN METHANOL SOLUTIONS

WŁODZIMIERZ BOCH

Chair of Acoustics, A. Mickiewicz University (Poznań)

Measurements of the ultrasonic velocity at 15 MHz and the density of $ZnCl_2$ solutions in methanol permitted determination of the dependence of the adiabatic compressibility of the solutions on temperature and concentration. The independence of the evaluated solvation numbers from the temperature and the insignificant decrease of their values with increasing solution concentration give evidence of the establishment in the solution of stable solvation complexes bound with complex ions $ZnCl_4^{2-}$.

1. Introduction

Electrolyte solutions are investigated by various physical methods including an acoustical technique. At the root of the acoustical method lies the unbalancing of the local thermodynamical equilibrium of the tested medium by the propagation of an acoustic wave.

Hydrous electrolyte solutions have been thouroughly investigated by the acoustical method and a great many papers [1] have been written on the subject. However, on the subject of electrolyte solutions in organic solvents there are only few papers available [2-7]. The aim of the work described in this paper is the determination of the effect of dissolved zinc chloride on the compressibility of methanol solutions and the evaluation of solvation numbers.

Methanol is a liquid strongly associated by hydrogen bonds. It can be generally assumed that methanol molecules may occur in the condensed phase in the structural configurations shown in Fig. 1. [17, 18].

The dissolution of any substance in methanol causes the destruction of the structure developed as a result of the binding the molecules by hydrogen bonds. In the case of electrolyte dissolution, the hydrogen bond cleavage occurs between methanol molecules, and this is followed by the specific action of ions upon the molecules of the solvent The effect of this action is the formation of certain configurations of methanol molecules around ions and electrolyte molecules known as solvation which in turn, brings about a stabilization of the solution structure.

BOCKRIS considers solvation to be a dual-natured process. Primary solvation is effected by the stabilization of certain dipole orientations of the solvent molecules around an ion and their binding with the ion as a result of the action of the ionic electrostatic field. This binding is so strong that the

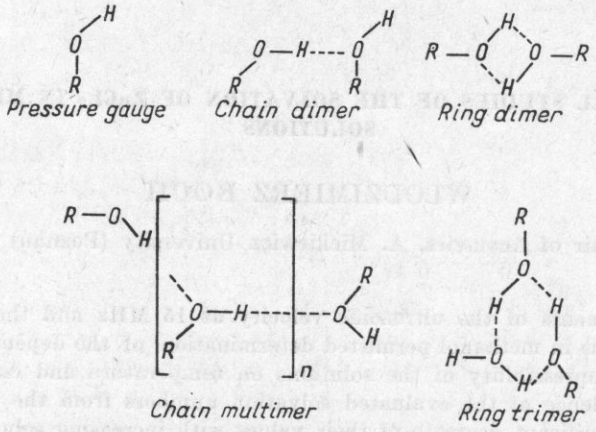

Fig. 1. Structural configurations of methyl alcohol

on in its translatory motions moves along with a solvation envelope. Secondary solvation consists in the polarization of further layers of the solvent and leads to a reduction in the dielectric constant in the region surrounding the ion, thus intensifying the action of the ion upon the solvent molecules.

Solvation resulting from the electrostatic action of the ionic electric field upon the solvent leads to a reduced compressibility of the solution [10-12]. The competitive effect is the destruction of the solvent structure by ions and electrolyte molecules introduced. This effect is primarily mechanical and depends on the size of the ions [13].

As a result of increasing the electrolyte concentration, the inter-ionic distances decrease and this permits the strong attraction of ions of opposite changes. In weak electrolytes the dissociation (ionization) decreases, while in strong electrolytes ions with opposite sign (gegenions) form a dipole, a pair of ions held together by electrostatic forces. In the limiting case, the ions partly lose their solvation envelopes and come into direct contact with each other, thus forming a contact pair of ions. The likelihood of the formation of pairs of ions increases with increasing electrolyte concentration.

Zinc chloride can exist in methanol solutions in the form determined by the following equation of equilibrium:

$$Zn^{2+}+2Cl^- \rightleftharpoons ZnCl_2,$$

$$2ZnCl_2 \rightleftharpoons ZnCl_4^{2-}+Zn^{2+},$$

$$ZnCl_4^{2-} \times Zn^{2+} \rightleftharpoons ZnCl_4^{2-}+Zn^{2+},$$

$$n\,ZnCl_4^{2-}+n\,Zn^{2+} \rightleftharpoons 2n\,ZnCl_2 \rightleftharpoons (ZnCl_2)_{2n}. \qquad (x)$$

A thorough study, chiefly using Raman spectroscopy has led to the conclusion [14-20] that in most cases zinc chloride occurs in methanol solutions in the forms determined by equilibrium (x), that is to say as ions Zn^{2+}, complex ions $ZnCl_4^{2-}$, complexes such as $ZnCl_2L_4$ or $ZnCl_2L_2$ (where L is the ligand of the solvent), and also in the form of quasi-polymer chains $(ZnCl_2)_{2n}$. The comparatively large number of forms in which zinc chloride occurs in solution is the reason for the considerable solvation effect which can be expressed as a changing of the adiabatic compressibility of the solutions.

The velocity of ultrasonic waves of infinitely small amplitude, i. e. such that the particle velocity amplitude in the wave is much less than the utlrasonic phase velocity, can be expressed via the density ϱ and the adiabatic compressibility coefficient β_s in the form of Laplace formula

$$c = \sqrt{\frac{1}{\varrho\beta_s}}. \tag{1}$$

The simultaneous measurement of the phase velocity of sound propagation and of the medium density permit univocal determination of the adiabatic compressibility using formula (1). At the present time this is the only method of determining, in a simple manner, the adiabatic compressibility of liquids.

The dissolution of the electrolyte changes the compressibility of the solvent mainly as a result of solvation. Proceeding from DEBYE'S considerations [21], PASYNSKI [22, 23] assumes that solvation complexes can be replaced by an effective solvated *volume* which is incompressible, while the compressibility of the remaining volume of the solution is equal to that of the pure solvent. It is thus possible to determine the solvation number, i. e. the number of molecules of solvent bonded with one electrolyte molecule, from the expression

$$Z = \frac{M}{M_0}\left(1 - \frac{\beta_s}{\beta_{s0}}\right)\frac{1-g}{g}, \tag{2}$$

where M is the molecular weight of the dissolved substance, M_0 — the molecular weight of the solvent, β_s — the adiabatic compressibility of the solution, β_{s0} — adiabatic compressibility of the solvent, and g — the liquid concentration by weight.

Determination of the adiabatic compressibility by the method mentioned above thus permits calculation of the solvation numbers.

2. Method and results of the investigations

The methanol used in the experiments was dehydrated by means of magnesium with a suitable addition of iodine and then distilled twice. The efficiency of the dehydration was tested with a small iodine crystal. The zinc chloride

used was dried for 18 hours at a temperature of 120°C. Substances prepared in these ways were used to make solutions with concentrations from 0.1 to 3.0 mol/l. The maximum error in the evaluation of the solution concentration was equal to 75×10^{-4} mol/l.

The measurements of the ultrasonic phase velocity were made at 15 MHz by means of an impulse-phase interferometer type UI-13, produced by IPPT PAN in Warsaw. To avoid evaporation of the solvent and, consequently, changes in the concentration of examined liquids, the measurement vessel was additionally sealed. The results of measurements of the ultrasonic velocity had a relative error not exceeding 2×10^{-3}.

The density of the liquids examined was determined by a picnometric method with an error of no more than 5×10^{-4}.

The temperature control system comprised the Höpler thermostat connected by rubber hoses to the measurement vessel. All parts of the system were additionally insulated thermally with a felt layer 15 mm thick. The liquids used for thermostatic control were the antifreeze «Borygo» at negative temperatures, and water at positive temperatures. The negative temperatures were obtained by the immersion of the thermostat in a vessel filled with a mixture of disintegrated solidified carbon dioxide (dry ice) and «Borygo» liquid. Temperature measurements were made with a graduated thermistor type ZE-3 operating in a Wheatstone bridge system. The temperature control system used permits evaluation of the temperature of an examined solution to an accuracy of 0.1°C. The temperature range of the measurements was from −20°C to 60°C.

The results of the measurements of ultrasonic velocity in solutions of zinc chloride in methanol are shown in Fig. 2.

From these measurements and those of solution density, the values of the adiabatic compressibility of the tested solutions were calculated. The results of these calculations are graphically represented in Figs. 3 and 4.

The dependence of the adiabatic compressibility on the temperature and the solution density has been thoroughly analyzed to find the analytical form of the functions $\beta_s = \beta_s(t)$ and $\beta_s = \beta_s(k)$. It was found that both functions are of exponential character. From the numerical calculations made for all concentrations it results that the functional formula $\beta_s = \beta_s(t)$ for a given solution concentration can take the form

$$\beta_s(t) = \underset{t=t_0}{\beta_s} \exp \mu(t-t_0), \quad k = \text{const}, \tag{3}$$

where $\beta_s(t)$ is the adiabatic compressibility at temperature t, $\underset{t=t_0}{\beta_s}$ is the adiabatic compressibility of the solution at the lowest temperature of measurement $t_0 = -20$°C, and μ is the temperature coefficient of the adiabatic compressibility of the solution.

Taking logarithms of the previous equation, we obtain

$$\log \beta_s(t) = \log \underset{t=t_0}{\beta_s} + \mu(t-t_0) \log e = \text{const} + (\mu \log e)t. \tag{4}$$

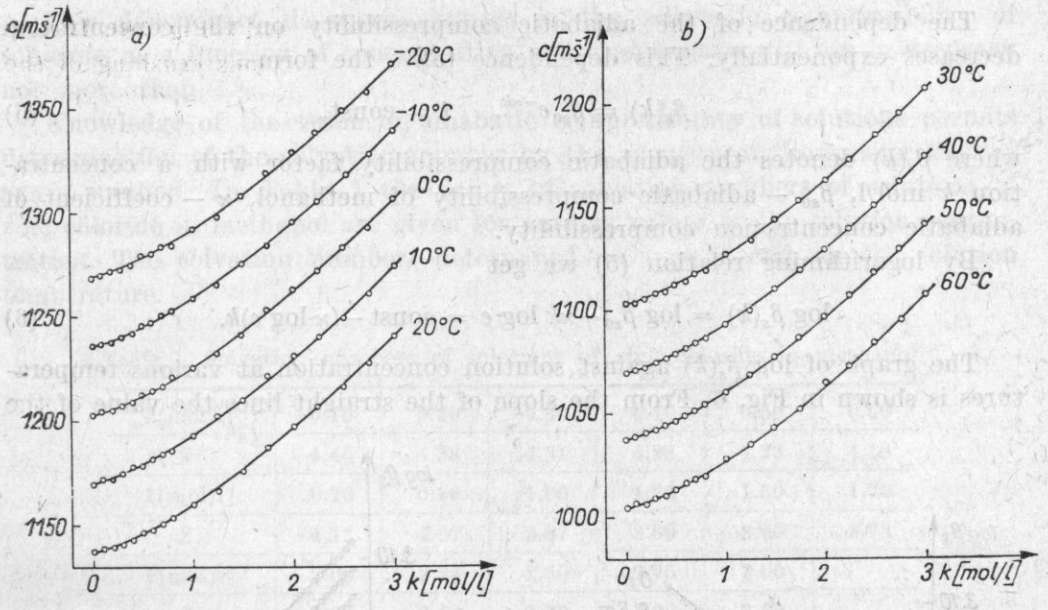

Fig. 2. Variation of ultrasound velocity with zinc chloride concentration for solutions in methanol

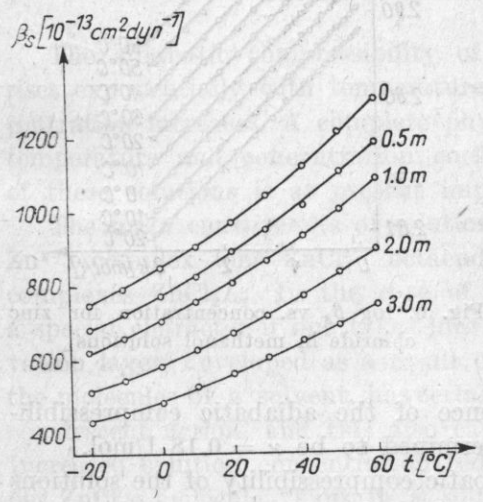

Fig. 3. Adiabatical compressibility vs. temperature for zinc chloride in methanol solutions with different concentrations

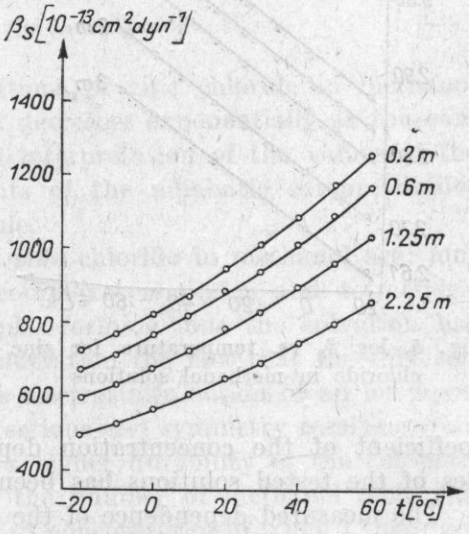

Fig. 4. Adiabatical compressibility vs. temperature for zinc chloride in methanol solutions with different concentrations

The value of the coefficient μ can be determined from the slope of the straight lines on the graph of log $\beta_s(t)$ against temperature (t). This dependence is shown in Fig. 5 for various solution concentrations. The value obtained from the graph for the temperature coefficient of the adiabatic compressibility of zinc chloride solutions in methanol has a value of $\mu = 68 \times 10^{-4} \mathrm{deg}^{-1}$.

The dependence of the adiabatic compressibility on the concentration decreases exponentially. This dependence takes the form

$$\beta_s(k) = \beta_{s0} e^{-\varkappa k}, \quad t = \text{const}, \tag{5}$$

where $\beta_s(k)$ denotes the adiabatic compressibility factor with a concentration k mol/l, β_{s0} – adiabatic compressibility of methanol, $\varkappa$ – coefficient of adiabatic concentration compressibility.

By logarithming relation (5) we get

$$\log \beta_s(k) = \log \beta_{s0} - \varkappa k \log e = \text{const} - (\varkappa \log e)k. \tag{6}$$

The graph of $\log \beta_s(k)$ against solution concentration at various temperatures is shown in Fig. 6. From the slope of the straight lines the value of the

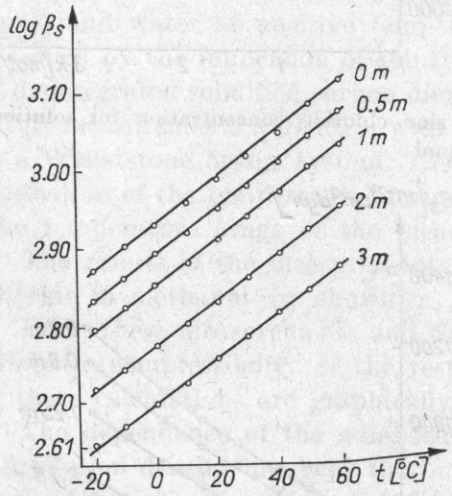

Fig. 5. $\log \beta_s$ vs. temperature for zinc chloride in methanol solutions

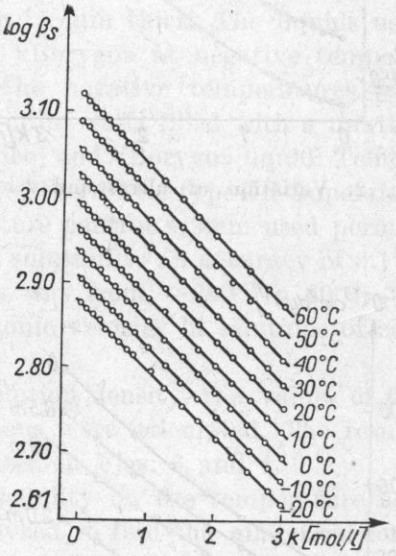

Fig. 6. $\log \beta_s$ vs. concentration for zinc chloride in methanol solutions

coefficient of the concentration dependence of the adiabatic compressibilities of the tested solutions has been determined to be $\varkappa = 0.18$ l/mol.

The measured dependence of the adiabatic compressibility of the solutions on the temperature and concentration can take one functional form for the range of concentrations and temperatures used in the investigations,

$$\beta_s(t, k) = \underset{t=t_0}{\beta_{s0}} \exp\left[\mu(t - t_0) - \varkappa k\right], \tag{7}$$

where β_{s0} is the adiabatical compressibility of methanol at a temperature $t_0 = -20°C$, and $\beta_s(t, k)$ – the adiabatic compressibility of a solution of concentration k mol/l at a temperature of $t°C$.

This dependence describes changes in the adiabatic compressibility of solutions as a function of concentration and temperature with an in accuracy not more than 1%.

Knowledge of the value of adiabatic compressibility of solutions permits determination of the solvation number by the acoustic method using PASYNSKY'S method. In Table 1 the values of solvation numbers of solutions of zinc chloride in methanol are given for various values of the solution concentration. The solvation numbers determined do not depend on the solution temperature.

Table 1. Solvation numbers of solutions of zinc chloride in methanol

k[mol/l]	0.10	0.20	0.30	0.40	0.50	0.60
Z	4.45	4.38	4.31	4.28	4.23	4.18
k[mol/l]	0.70	0.80	1.00	1.25	1.50	1.75
Z	4.13	4.07	3.97	3.89	3.80	3.73
k[mol/l]	2.00	2.25	2.50	2.75	3.00	
Z	3.64	3.50	3.39	3.29	3.20	

3. Analysis of results of the investigation

The adiabatic compressibility of solutions of zinc chloride in methanol rises exponentially with temperature and decreases exponentially as the concentration increases. A complete physical interpretation of the values of the temperature and concentration coefficients of the adiabatic compressibility of these solutions is at present impossible.

The main constituents of solutions of zinc chloride in methanol are: ions Zn^{2+}, complex ions $ZnCl_4^{2-}$ octaendric complexes $ZnCl_2L_4$, and tetraendric complexes $ZnCl_2L_2$. In the case of complex-forming ions the solvation has a special character if one takes into consideration the fact that the first solvation layer, developed as a result of the electrostatic action of an ion upon the molecules of a solvent, has certain directions and symmetry resulting from covalescent action, and this also causes a higher durability of the complex. Increased solution concentration reduces the number of methanol molecules per $ZnCl_2$ - molecule. Thus in a solution of concentration 0.1 mol/l there are 247 methanol molecules per $ZnCl_2$ - molecule, while in a solution with concentration 3.0 mol/l there are only 8 methanol molecules. Such a considerable change in the ratio of the numbers of molecules does not, however, effect an equally considerable change on the solvation numbers.

The solvation number varies from 4.45 for a concentration of 0.1 mol/l to 3.20 for a concentration of 3.0 mol/l, having an average value of 4. Such an insignificant change of the solvation number is an explicit proof of the

establishment in the solution of very durable solvation complexes. The negligible decrease of the solvation number with increasing solution concentration results only from the «competitive» action of the ions in methanol molecule binding in the solvation envelope, since the relative number of these molecules decreases considerably with increasing solution concentration. The independence of the solvation number from the temperature also evidences the considerable durability of the developing solvatation complexes. The intensification of the thermal motion of the methanol molecules (the ions) with increasing temperature does not cause any change in the solvation numbers.

It seems that the complex ions $ZnCl_4^{2-}$ predominate in the solvatation process. This conception is supported by the independence of the solvation numbers from the temperature (complex ions development very stable solvatation complex) and by the fact that the value of the solvation number is about 4. This would suggest that a complex ion binds four methanol molecules in quasi-hydrogen bonds. The share of other forms of zinc chloride, encountered in the solution in the solvation process, seems to be negligible. The ions Zn^{2+}, on one hand, act electrostatically upon the methanol molecules, while, on the other hand, being large ions, destroy the mechanical structure of the methanol. Both effects are competitive effects and seem to bring about a total insignificant effect in the solvatation process.

References

[1] L. Bergmann, *Der Ultraschall und seine Anwendung in Wissenschaft und Technik*, Zürich 1954.

[2] M. J. Blandamer, D. E. Clarke, N. J. Hidden, M. C. R. Symons, Trans. Faraday Soc., 64, 1193 (1968).

[3] S. Petrucci, M. Battistini, J. Physic. Chem., 71, 1181 (1967).

[4] S. Petrucci, G. Atkinson, Physic. Chem., 70, 2550 (1966).

[5] S. Petrucci, F. Fitipaldi, J. Physic. Chem., 71, 3087 (1967).

[6] M. J. Blandamer, M. J. Foster, N. J. Hidden, M. C. R. Symons, J. Physic. Chem., 72, 2268 (1968).

[7] A. Z. Golik, O. W. Tarasenko, P. F. Czołpan, Akust. Żurn., 20, 33 (1974).

[8] F. A. Smith, E. C. Creitz, J. Research Nat. Bur. Standards, 46, 145 (1951).

[9] M. Van Thiel, E. D. Becker, G. C. Pimentel, J. Chem. Phys., 27, 95 (1957).

[10] F. Gucker, Chem. Rev., 13, 111 (1933).

[11] C. Bachem, Zs. Phys. 101, 541 (1936).

[12] S. Subrahmanyam, Zs. Phys. Chem. Leipzig, 5, 219 (1962).

[13] E. Ganz, Zs. Phys. Chem., B 35, 1 (1937).

[14] R. A. Robinson, R. H. Stokes, *Electrolyte Solutions*, Butterworths Sciences Public., London 1959.

[15] *Spectral investigation of the structure of electrolytes* (collective work), PWN, Warszawa 1969 [in Polish].

[16] C. S. Venkateswaran, Proc. Ind. Acad. Sci., A. 1, 850 (1935).

[17] M. L. DELWAULLE, Bull. Soc. Chim. France, 1294 (1955).
[18] H. R. OSWALD, H. JAGGI, Helv. Chim. Acta, 43, 72 (1960).
[19] A. C. HARRIS, H. N. PARTON, Trans. Faraday Soc., 36, 1139 (1940).
[20] R. H. STOKES, Trans. Faraday Soc., 44, 137 (1948).
[21] P. DEBYE, *Kompressibilität von Ionenlösungen*. Festschrift Heinrich Zangger, II, Zürich-Leipzig-Stuttgart, 877 (1935).
[22] A. PASYNSKI, Żurn. Fiz. Chim., 20, 981 (1946).
[23] A. PASYNSKI, Żurn. Fiz. Chim. 11, 606 (1938).

Received on 22nd May 1976

ARCHIVES OF ACOUSTICS
2, 1, 35-45 (1977)

ACOUSTIC MEASUREMENT OF THE SHEAR COMPLIANCE OF SILICONE OIL

RYSZARD PŁOWIEC

Institute of Fundamental Technical Research
Polish Academy of Sciences (Warszawa)

A method of measurement is described and the results of measurement of the modulus limit shear compliance J_∞ of four samples of synthetic oil with different molecular weight compared. Oil properties have been measured acoustically by determining the characteristic shear resistance at a stress frequency of 30 MHz and 450 MHz and in the temperature range from 0°C to −100°C.

It was found that the increase of molecular weight has only little influence on the limit of the modulus of shear compliance of the liquid.

1. Introduction

It is a well known fact that viscosity characterizes a liquid medium only in the case of its distortion at comparatively low frequencies. As the liquid is subjected to distortions of increasing frequency its (dynamic) viscosity decreases while the liquid shear modulus of elasticity (G) increases. At very high frequencies the dynamic liquid viscosity decreases to zero while the shear modulus of elasticity asymptotically approaches a large value (the limiting value, G_∞). Furthermore, it was found that this limit of the liquid of the modulus of elasticity G_∞ is of the same order of magnitude as the modulus of elasticity of a solid.

The phenomenon of decreasing dynamic viscosity and increasing elasticity of a medium plays an essential role in lubrication, thus much attention has been devoted to measurements of this kind [1, 2].

The modulus of shear elasticity of a liquid G_∞ or the commonly used modulus of the shear compliance of a liquid J_∞ ($J_\infty = 1/G_\infty$) is an interesting quantity from the molecular viewpoint since it supplies information on the ability of molecules to perform the translational or rotational motions encountered in the lubrication process [3].

In these investigations an important role is played by ultrasonic and hypersonic vibrations which permit the production in the examined liquids of shearing stresses with a distortion frequency of over 10^9 Hz [4].

The reaction of a liquid to shearing stresses is determined acoustically by measuring the so-called characteristic shear impedance Z which is the ratio of the shearing stress (in dyn/cm^2) to the velocity of a molecule (in cm/s). Theoretically, the liquid reaction can be determined comparatively easily on the basis of a network model of liquid medium, which is valid for the propagation of plane shear waves [14]. For solids the characteristic impedance is a real magnitude and is given by

$$Z = \varrho C_T = \sqrt{\varrho G},$$

where ϱ is the density of the medium, C_T – the velocity of propagation of transverse waves in the medium and G – the shear modulus of elasticity.

In the case of viscoelastic liquids the shear impedance is a compound quantity ($Z_c^* = R_c + jX_c$), as also is the shear modulus ($G^* = G' + jG''$), thus

$$Z_c^* = \sqrt{\varrho G^*}.$$

With a sufficiently high frequency the imaginary component of the impedance (X_c) is considerably smaller than the real component (R_c) and in this range it can practically be neglected. Thus the limiting, high-frequency shear modulus of elasticity is

$$G_\infty = R_c^2/\varrho. \tag{1}$$

When determining the absolute value of the limiting value of the shear modulus of elasticity by the acoustic method, it is also necessary to know the density of the examined medium. It is determined using one of the known physical methods.

The frequency of the distortions which should be induced in the liquid to determine the limiting value G_∞ is dependent upon the type of sample examined. This frequency should be considerably higher than that of viscoelastic relaxation f_0, the time of this relaxation $\tau(\tau = 1/f_0)$ being given by

$$\tau = \eta/G_\infty,$$

where η is the static viscosity of the examined sample. The value of the modulus G_∞ is very similar for individual liquids (Fig. 9), so that the frequency of the distortions, for example for a liquid sample with a viscosity of about 0.01 $N \times s \times m^{-2}$ (10 cP), should be higher than 10^{10} Hz. With present techniques it is possible to test liquids at frequencies up to 10^9 Hz. Thus to determine the limiting shear elasticity of a liquid with a low viscosity, the measurements are made of necessity at reduced temperatures. For such investigations liquids are selected which can be supercooled and are thus capable of giving very high viscosities and a clearly defined range of pure elasticity.

The measurements described below are made at reduced temperatures, from 0 to −100°C, with samples from four types of a synthetic oil at two measuring frequencies 30 MHz and 450 MHz, to investigate the effect of the molecular weight on the limiting value of the shear compliance.

2. Acoustic determination of shear resistance

The characteristic value of the impedance of a liquid can be best evaluated by measuring the coefficient of reflection of ultrasonic waves at the boundary of two media of which one is a known medium and the other the liquid to be examined. Crystalline or fused quartz, for which the shear impedance Z_q and its dependence temperature are known, is used for the former medium.

To measure the coefficient of reflection k by means of a quartz transducer a pulse of vibrations is set up on the cylindrical surface of a fused quartz delay line. A suitable cut of the transducer provides a pulse of transverse vibrations with a polarisation perpendicular to the direction of wave propagation. This pulse, which propagates along the delay line, will be reflected from the surface opposite the transducer. Should this surface be in air, the reflection of the pulse ($k = 1$) will be virtually complete, but if the surface is located in a liquid, the coefficient of reflexion will be [5]

$$k = \frac{Z_c - Z_q}{Z_c + Z_q}. \tag{2}$$

The very high damping of transverse waves in liquids means that formula (2) is valid even for a comparatively thin layer of liquid on the surface of the delay line.

Within the elastic range of a liquid where $X_c = 0$, and also when $X_c \ll R_c$, formula (2) can be written as

$$R_c = Z_q \frac{1-k}{1+k}, \tag{3}$$

where k is the ratio of the voltages of the signals that correspond to the reflected and incident pulses.

3. The characteristics of the examined liquids

The liquid used for the investigations was a synthetic oil, trifluoropropyl methylsiloxane (FS 1265), produced by the British firm Midland Silicone Limited. This liquid is a linear polymer, free of main chain branches. Four samples of this liquid with different lengths of the chain were examined. The static viscosity of the different types at room temperature (20°C) and their mean molecular weights ($\bar{M}_n$) are stated below:

Sample	η	$\bar{M}_n$
A	1,72 P (0.172 N.s.m.$^{-2}$)	1720
B	30,0 P (3.0 N.s.m.$^{-2}$)	9050
C	179,0 P (17.9 N.s.m.$^{-2}$)	20000
D	8120,0 P (812.0 N.s.m.$^{-2}$)	72600

4. Measuring system

The diagram of the measuring system is shown in Fig. 1. The operation of the system is controlled by square impulse generator (*1*) which modulates the oscillator at a frequency of 200 Hz to obtain vibrations at this frequency from the impulse transmitter. These impulses then induce transverse vibra-

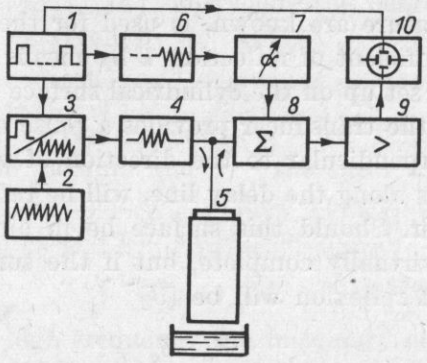

Fig. 1. Diagram of measurement system

1 – square pulse generator, *2* – continuous wave generator (oscillator), 3 – modulator, *4* – h.f. pulse transmitter, *5* – transducer, *6* – comparative pulse generator, *7* – regulating attenuator, *8* – totalizing system, *9* – amplifier, *10* – oscilloscope

tions on the quartz transducer (*5*) with BT cut. The induced vibrations are propagated along the cylindrical delay line made of fused quartz. The impulses, after being reflected from the opposite end of the line, are received by the same transducer which acts as a receiving transducer at times between the transmitted impulses. The received impulses are then amplified (*9*) and, after detection, visualized on an oscilloscope screen (*10*).

To measure the amplitude of a received signal an auxiliary transmitter (*6*) of the same frequency is impulse-modulated with a short delay in relation to the main transmitter. The output signal from the auxiliary transmitter is passed through an attenuator (*7*) with precise and continuous attenuation control to meet in the totalizing system with the received signal. Both signals are then amplified and, after detection, visualized on the oscilloscope screen. The delay of the auxiliary impulse is controlled in such a manner that both impulses, received and auxiliary, are very near to each other. The latter can then be easily reduced to the same amplitude as the former by means of the attenuator (*7*). To increase the measurement accuracy advantage is taken of signals reflected repeatedly from the delay line. The coefficient of reflection k is determined from the difference in the attenuation of consecutive echoes for air (q_p) and for the examined liquid (q_c),

$$k = q_p/q_c,$$

where $q = A_n/A_{n+1}$, A_n and A_{n+1} denote the amplitudes of consecutive impulse reflections.

A measuring system operating on a similar principle has been used at a frequency of 450 MHz with only a quartz crystal being used in direct contact with the liquid. This crystal has been iduced to emit transverse vibrations in a special resonance cavity by the method described in a previous publication [6].

5. Measurement results

The measurements of the density of liquid samples as a function of temperature were made by means of a pycnometer. The measurement error of the liquid density by this method is estimated to be $\pm 0.1\,\%$. The density of each sample for about 10 different temperatures within the range from $-70°C$ to $50°C$ has been determined.

For all measured temperatures linear dependence of density on temperature was found to exist within the investigated temperature range, in agreement with the equation

$$\varrho_{(T)} = \varrho_0[1-\alpha_0(T-T_0)] \ [\mathrm{g/cm^3}]. \tag{4}$$

Table 1. Values of the parameters of the density, eq. (4)

Specimen	ϱ_0	$\alpha_0(\times 10^4)$	T_0[K]
A	1.3515	7.4	151.6
B	1.3707	5.83	156.0
C	1.3945	6.02	163.0
D	1.4315	6.99	166.6

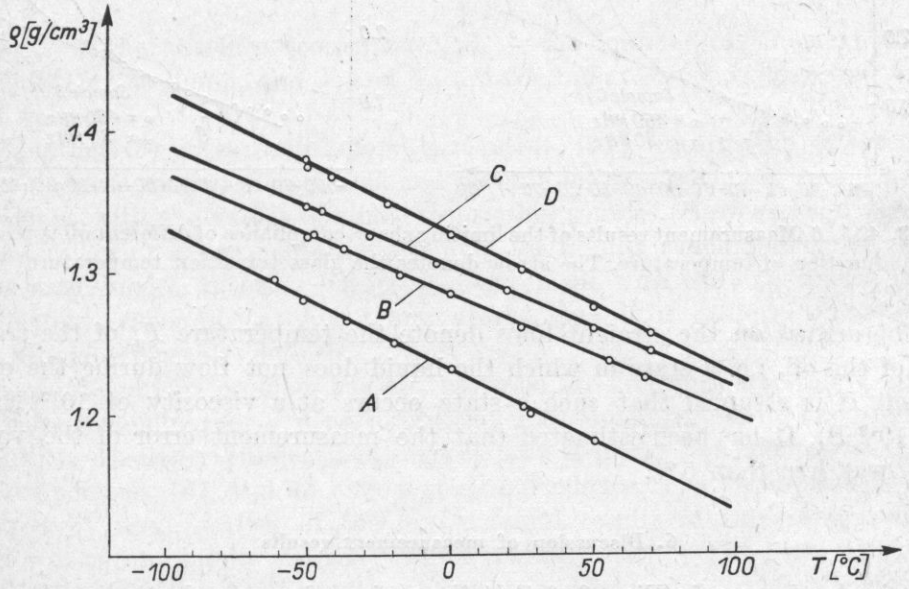

Fig. 2. Variations of the density of the liquids tested as a function of temperature

The values ϱ_0, α_0 and T_0 for individual liquid types are given in Table 1.

The measurement points and equation (4) for $\varrho_{(T)}$ have been plotted in Fig. 2 for the different samples of liquid. Measurements of shear resistance R_c at different temperatures within the range from 0 to $-100°C$ and at frequencies of 30 MHz and 450 MHz were made by the method described above. During the measurement the temperature was controlled by means of a platinum resistance thermometer with an accuracy of $\pm 0.1°C$.

The measurement results in the form of quotient ϱ/R_c^2, being the liquid shear compliance, J_∞, are shown for the different samples in Figs. 3-6.

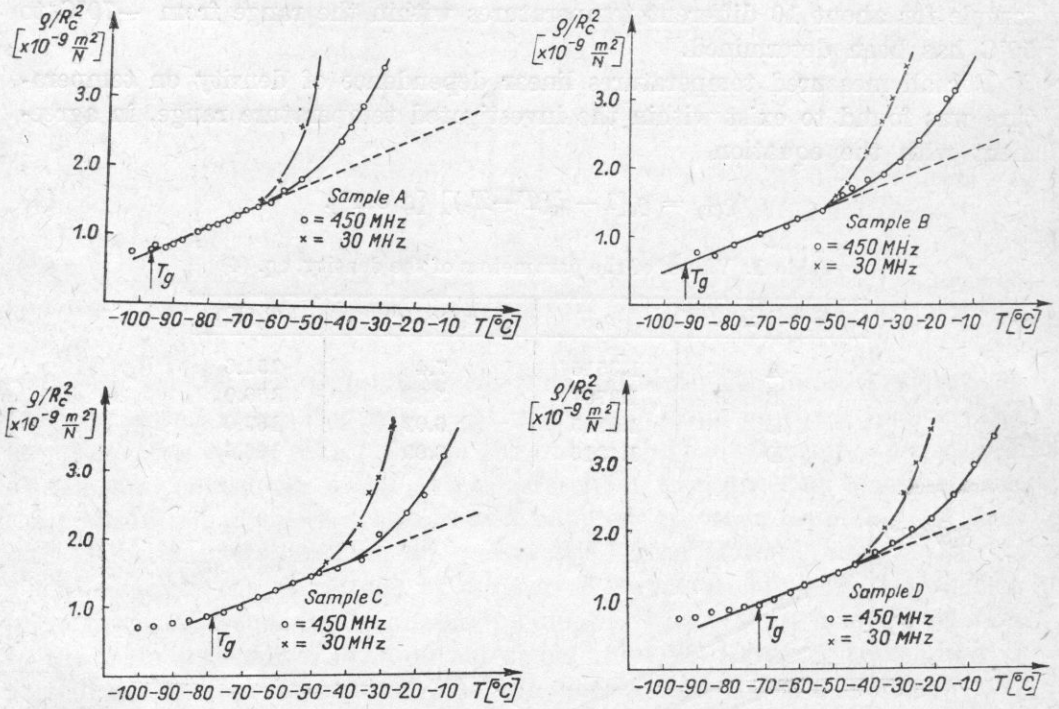

Fig. 3, 4, 5, 6. Measurement results of the limiting shear compliance of different oil types as a function of temperature. The arrow denotes the glass transition temperature

The arrows on the straight lines denote the temperature T_g of the transition of the oil, i.e. a state in which the liquid does not flow during the experiment. It is assumed that such a state occurs at a viscosity of 10^{12} Ns/m^2 (i.e. 10^{13} P). It has been estimated that the measurement error of the values of R_c was less than 5%.

6. Discussion of measurement results

It is clearly seen in Figs. 3-6 that the region of purely elastic liquid occurs in a comparatively narrow temperature range, between the temperature (T_g) of the glass transition of the liquid and the temperature at which the

viscoelastic relaxation predominates. Within this range the quotient ϱ/R_c^2 has the same value both for frequencies 30 MHz and 450 MHz. The constant value of the quotient ϱ/R_c^2 for various frequencies confirms the occurrence in the liquid of the elastic range. For this reason, in order to separate the elastic range from the relaxation range and to evaluate the temperature dependence of the limiting compliance J_∞, it is necessary to use at least two frequencies for the measurement.

The literature contains many papers dedicated to calculating G_∞ or J_∞ or describe their dependence on the temperature. For instance, for hydrogen-bonded liquids the dependence

$$J_\infty = J_\infty^0 + \frac{BV}{n_H N}\left[\exp\left(-\frac{\Delta H}{RT}+\frac{\Delta S}{R}\right)+\frac{V_f}{V}\right] \tag{5}$$

has been derived [12], where J_∞^0 is the magnitude of the limiting elasticity which is characteristic for glassy liquids, B is a constant for a given liquid, V – the molar liquid volume, n_H – the number of hydroxide groups per molecule, N – Avogadro's number, R – the ideal gas constant, and ΔH and ΔS – quantities required for the description of the temperature and pressure dependencies. On the other hand, REE, REE and EYRING [15] have derived for the limiting liquid shear elasticity the formula

$$G_\infty = \frac{6RT}{2Z_n(V-V_0)}, \tag{6}$$

where T is the absolute temperature, Z_n – the number of the next closest molecules in the liquid, and V and V_0 are the molar liquid volume and molar solid volume.

Equation (5) gives satisfactory agreement [13] within the supercooled range and the magnitudes of ΔH and ΔS for many associated liquids are in agreement with the values obtained from other sources. However equation (6) agrees well with experimental results only for liquids which satisfy Maxwell's viscoelastic model. In other liquids the agreement with the experiment is not satisfactory, especially at low temperatures, and it is at low temperatures that G_∞ is preferably defined.

A quite complex problem has proved to be the description of the nature of the variations in G_∞ (or J_∞) as a function of temperature from experimental results [7, 8]. Other publications suggest both a linear dependence of G_∞ on the temperature [8], and an exponential dependence. The description is complicated by some scatter of the experimental results in this comparatively narrow range of liquid elasticity which permits both possibilities of dependence. The reason for the considerable scatter of the measurement points are the technical limitations of making an accurate measurement of the resistance of a liquid and its temperature.

Latterly in the literature the notion of a linear dependence of J_∞ on the temperatures has prevaited, as described by the formula [10]

$$J_\infty = \frac{1}{G_\infty} = \frac{1}{G_\infty^0}[1+B(T-T_0)]. \tag{7}$$

This dependence is entirely empirical, but it proves its practicability exceptionally well when compared with the results of measurements at various temperatures and frequencies [11]. It may be assumed that the above form for J_∞ as a function of temperature is connected with the variation of a free liquid volume $V_f = V - V_0$, where V is the characteristic volume equal to $1/\varrho$, $V_0(1/\varrho_0)$ is the packing volume of molecules encountered in the vitreous state at the temperature T_0.

The linear dependence of J_∞ on the temperature may be expected to occur when the density of the tested liquid has a linear temperature dependence as described by equation (4). The free liquid volume is in this case

$$V_f = \frac{\varrho_0 - \varrho}{\varrho_0 \varrho} = \alpha_0 V(T-T_0),$$

where α_0 is the coefficient of expansion at the temperature T_0 and is defined in Table 1. Substituting this into equation (7), the approximate formula for the limiting liquid shear compliance can be written [8]

$$\frac{1}{G_\infty} \cong \frac{1}{G_\infty^0} + \frac{\alpha_0}{G_1}(T-T_0). \tag{8}$$

The approximation covers the range $G_\infty^0 \gg G_1$, where $1/G_1$ is the compliance connected with the relaxation of the structure and the appearance of a free volume.

The dependence of G_∞ and J_∞ on the free liquid volume also occurs in equations (5) and (6). In the absence of hydrogen bonds in the liquid equation (5) can be reduced to equation (7).

The comparison of the results of measurement on different oil samples at various temperatures and frequencies has assisted in finding a linear dependence for the variation of J_∞ with temperature. This variation is represented in Figs. 4-6.

Table 2 states the magnitudes of J_∞^0, B and T_0 evaluated from equation (7) for the different oil types.

Table 2. Values of the parameters of the rigidity modulus, eq. (7)

Specimen	$\frac{1}{G_\infty^0}$ [$10^9 m^2/N$]	β	T_0[K]
A	0.2	0.112	151.6
B	0.154	0.125	156.0
C	0.297	0.0627	163.0
D	0.331	0.057	166.6

In this manner the range of variations of the limiting shear compliance as described by formula (7) and shown in Figs. 3-6 can be divided into two regions:

a) the region over which J_∞ is measured directly where the experimental results obtained confirm the validity of equation (7) (continuous line in Figs. 3-6),

b) the region over which J_∞ cannot be measured directly because of the predominant effect of the viscoelastic relaxation. In this region an extrapolation is used – which agrees with formula (7) – to determine the value of J_∞ within the relaxation range (broken line in Figs. 3-6).

A comparison of the measurement results of the limiting shear compliance and its temperature dependence for the liquid samples tested is shown in Fig. 7. It can be seen that differences in the limiting value of the shear compliance for types B, C and D are insignificant in spite of a considerable difference in the static viscosity of these samples.

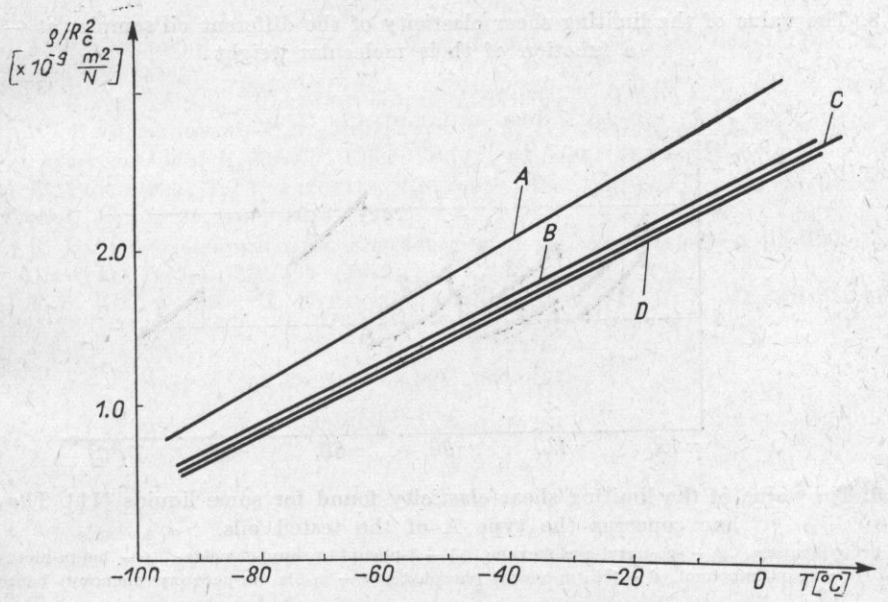

Fig. 7. Comparison of the variation of the limiting shear compliance with temperature for the different oil samples

The value of the limiting shear elasticity exhibited by the samples at a temperature of −80°C as a function of their mean molecular weight $\bar{M}_n$ is shown in Fig. 8. It can be seen that the molecular weight has an insignificant effect on the limiting modulus G_∞. Despite large differences in the molecular weight between the samples the values of G_∞ vary within comparatively narrow limits $(0.9\text{-}1.25)\times 10^9$ N/m².

Fig. 9 shows the values of G_∞ in the neighbourhood of the glass transition temperature of the various liquids and their variation with temperature as

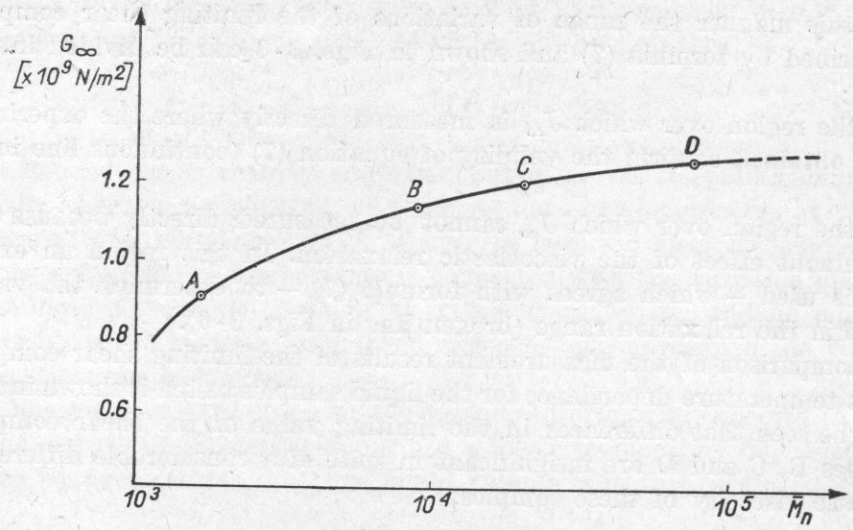

Fig. 8. The value of the limiting shear elasticity of the different oil samples at −80°C as a function of their molecular weight

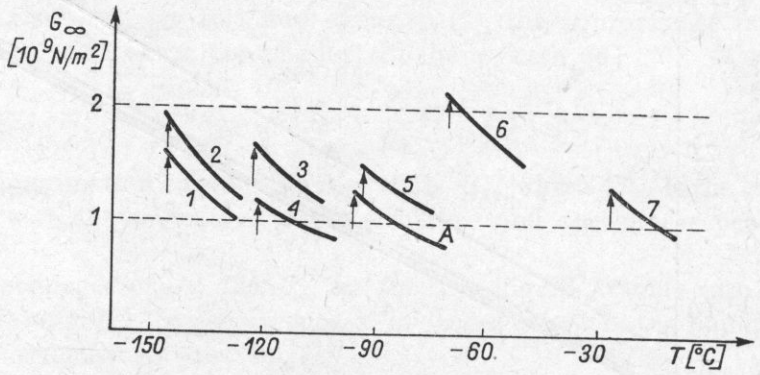

Fig. 9. The value of the limiting shear elasticity found for some liquids [11]. The broken line concerns the type A of the tested oils

1 — n-propylbenzene, *2* — sec-butyl-cyclohexane, *3* — 3-phenyl propyl-chloride, *4* — hepta-methylnonane *5* — 3-phenyl propanol, *6* — tri (m-cresyl) phosphate, *7* — m-bis (m-phenoxy phenoxy) benzene

quoted by other authors [11]. It is worth noting also that in spite of a large differentiation of the liquids compared in Fig. 9 (simple and polymer liquids) the absolute values of the limiting shear elasticity G_∞ in the vicinity of the vitrification temperature are approximatly the same, being within the limits $(1\text{-}2)\times 10^9$ N/m^2.

Acknowledgment. The measurements described were performed during the author's post-graduation scientific practice at the University of Glasgow (G. Britain). The author is anxious to express his gratitude to Prof. J. LAMB for his contribution in enabling these measurements to be performed.

References

[1] *Molecular and non-linear acoustics*, [in Polish] Collective Works, Polish Academy of Sciences, 1956.

[2] J. D. Ferry, *Viscoelasticity of polymers*, WNT, Warszawa 1965 [in Polish].

[3] K. Osaki, *Viscoelastic properties of dilute polymer solution*, Advances in Polymer Science, 12, 1-64 (1973).

[4] R. Płowiec, *On the possibility of ultrasonic investigations of viscoelastic properties of liquids* [in Polish], Polimery, 2, 27-72 (1967).

[5] J. Wehr, *Measurements of the velocity and attenuation of ultrasonic waves* [in Polish], PWN, Warszawa 1972.

[6] R. Płowiec, *Measurement of viscoelasticity shear properties of liquids at distortion frequencies of the order of 1000 MHz* [in Polish], Archiwum Akustyki, **5**, 4, 411-419 (1970).

[7] W. M. Slie, A. R. Donfor, T. A. Litovitz, *Ultrasonic shear and longitudinal measurements in aqueous glycerol*, J. Chem. Phys., 44, 3712-3718 (1966).

[8] A. J. Barlow, J. Lamb, A. J. Matheson, P.R.K.L. Padmini, J. Richter, *Viscoelastic relaxation of supercooled liquids*, Proc. Roy. Soc. A2 98, 467-480 (1967).

[9] G. J. Gruber, T. A. Litovitz, *Shear and structure relaxation in molten zinc chloride*, J. Chem. Phys., 40, 13-26 (1964).

[10] A. J. Barlow, J. Lamb, *Viscoelastic relaxation of supercooled liquids*, Disc. Farad. Soc., 43, 223-230 (1967).

[11] A. J. Matheson, *Molecular acoustics*, Wiley – Interscience, 1971.

[12] W. M. Madagosky, G. E. McDuffie, T. A. Litovitz, *Free volume of shear compliance of hydrogenbonded liquids*, J. Chem. Phys., 47, 753-757 (1967).

[13] R. Piccirelli, T. A. Litovitz, *Ultrasonic shear and compressional relaxation in liquid glycerol*, JASA, **29**, 1009-1018 (1957).

[14] R. Płowiec, *Characteristic impedance of a viscoelastic medium* [in Polish], Archivum Akustyki, **7**, 3-4, 353-368 (1972).

[15] T. S. Ree, T. Ree, H. Eyring, Proc. Nat. Acad. Sci. U. S., **48**, 501-510 (1962).

Received on 8th May 1975

Revised 15 Juni 1976

ARCHIVES OF ACOUSTICS
2, 1, 47-70 (1977)

PHYSICAL MODELS OF THE LARYNX SOURCE

JANUSZ KACPROWSKI

Department of Cybernetic Acoustics, Institute of Fundamental Technological Research
Polish Academy of Sciences (Warszawa)

The development of objective acoustic methods in the medical diagnostics of several speech disorders and the resulting clinical applications in laryngology and phoniatry call for a versatile physical model of the human larynx source. Such a model should simulate the physiological structure and the characteristics of the natural, i.e. biological laryngeal system from both the phenomenological and the quantitative points of view. In the present paper the performance and the general characteristics of the human larynx source are briefly described and its acoustic parameters are defined. Special attention is paid to the physical meaning of these parameters and to the parallels which exist between them and the anatomical structure of the biological system. On the basis of a few rationally motivated simplifying assumptions the mechanical model of the human larynx source and its equivalent electrical analogue circuit are described and discussed. Special attention is paid to the two-mass model which is very convenient for diagnostic purposes. The physical interpretation of the model's acoustic parameters is given and its mathematical description is formulated, the latter being expressed in the form of two sets of differential equations, describing air-flow and mass-movement, respectively. Finally, the convenience and the usefulness of the model in application to laryngological and phoniatric diagnostics of larynx disorders is briefly discussed and validated.

1. Introduction

The biological larynx generator, which is the only source of energy in the articulation of vowels and nasal consonants, and the main source of energy in the articulation of all remaining voiced speech sounds, plays a fundamental rôle in the process of conveying information by means of speech. It affects both the *linguistic information* which is responsible for the phonemic and the semantic content of the conveyed message, and the *personal information* which describes the individual features of the speaker's voice. Since the larynx source not only enables the correct articulation of all voiced sounds, but also is responsible for several suprasegmental prosodic features of speech, such as intonation, melody, accent and duration, it is evident that a knowledge of the mechanism of its action as well as of the relations that exist between its acoustic parameters and the anatomical structure of the source itself is necessary

both for programmed speech synthesis in technical systems, e.g. in computers, and in medical diagnostics and/or in rehabilitation of speech disorders. The latter application is of particular importance since the pathology and the anomalies of the larynx constitute a very high proportion of problems in laryngology and phoniatry. It concerns both congenital and developmental defects, defects caused by professional diseases and those arising from necessary surgical intervention, viz. laryngotomy and tracheotomy.

Acoustic diagnostic methods in laryngology and phoniatry, which are based, generally speaking, on an analysis of the information content of the speech signal as the final and natural output from the speech—organs, have recently become commonly used in clinical practice (cf.e.g. [14]). They not only assist, but in some cases are even superior to the prior classical methods, e.g. laryngoscopy, stroboscopy, electromyography and radiography etc., since:

— they are used under normal conditions of phonation and articulation,

— they neither need any surgical tool or foreign substances to be introduced into the speech organ, nor have to be aided by any dangerous and painful, intrusive procedures,

— they enable the real-time visualization of the acoustic parameters of the speech signal, e.g. on TV monitor. They are thus especially convenient during rehabilitation since the hearing disorders, usually associated with speech disorders, may be compensated by the additional and auxiliary information channel of the sight organ.

Acoustical methods consist, generally, in the measurement and analysis of those acoustical parameters of the speech signal which describe the internal structure of the respective sound source, in laryngeal diagnostics the larynx generator [13]. The development and application of these methods in clinical practice must be supported by a versatile physical model of the human larynx source, a model that can simulate the action and the characteristics of the natural biological system not only in qualitative, but also in quantitative terms.

2. The mechanism of action and the general characteristics of the larynx source

2.1. *The principles of action and the physical parameters of the larynx source.* Fig. 1 represents the anatomical structure of the human larynx. The larynx source may be considered from a physical point of view as an aerodynamic oscillator whose behaviour is determined by some physical parameters (such as subglottal pressure and mechano-acoustical or structural constants of the vocal folds) and also to some extent depends on the acoustic load represented by the input impedance of the vocal tract. In the general case this tract consists of the pharynx, mouth and nasal cavities. The action of this oscillator must be considered in close connection with that of the subglottal part of the human respiratory system, which is shown in Fig. 2 in the form of a simplified

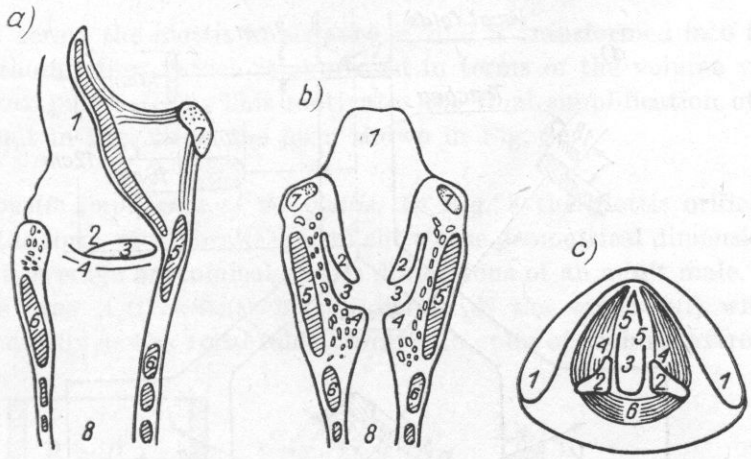

Fig. 1. Anatomical structure of the human larynx [16]

a) profile cross-section: *1* – epiglottis, *2* – false vocal fold, *3* – ventricle of Morgagni, *4* – vocal fold, *5* – thyroid cartilage, *6* – cricoid cartilage, *7* – hyoid bone, *8* – trachea; b) frontal cross-section (notations as above); c) horizontal cross-section: *1* – thyroid cartilage, *2* – arytenoid cartilages, *3* – glottis, *4* – vocalis muscles, *5* – vocal ligaments, *6* – transverse arytenoid muscles

physical model and its two equivalent electrical circuits in the impedance--type system of analogy.

The vocal folds, having a definite mass m, stiffness s and loss-resistance r, are set in forced vibrations by the local pressure variations in the glottis. This pressure variations are caused by the flow of air which is expelled from the lungs through the bronchi and trachea by the muscle forces of the rib-cage (thorax), acting on the lung tanks. The flow of air out of the lungs is – at constant voice effort – an isobaric process since the lungs volume $V = V' + V''$ (Fig. 2a), represented in Fig. 2b by the condenser C_L, decreases as the quantity of air in the lungs diminishes, so that the relation of the charge Q_L to the capacity C_L (i.e. the voltage $U_L = Q_L/C_L$ on the equivalent condenser C_L) remains constant. It follows that the air pressure P_L in the lungs corresponding to the voltage U_L also remains constant, i.e. $P_L = \text{const}$. The larynx generator may thus be considered in future discussions and equivalent electric circuits as a system which is driven by voltage source of constant electromotive force $P_L = \text{const}$ with zero internal impedance. This has been shown in Fig. 2c, where the conductance G_L of the condenser C_L, representing the negligible acoustic loss resistance of the spongy and vesicular walls of the lung tanks has been disregarded.

The quasi-periodic vibrations of the vocal folds change the acoustic impedance $Z_g = R_g + j\omega L_g$ of the glottis modulating the air flow. At the entrance to the vocal tract the air flow has the form of recurrent discrete pulses. The latter play the rôle of an impulse source function, which excites vibrations of the air in the vocal tract at frequencies corresponding to the resonances

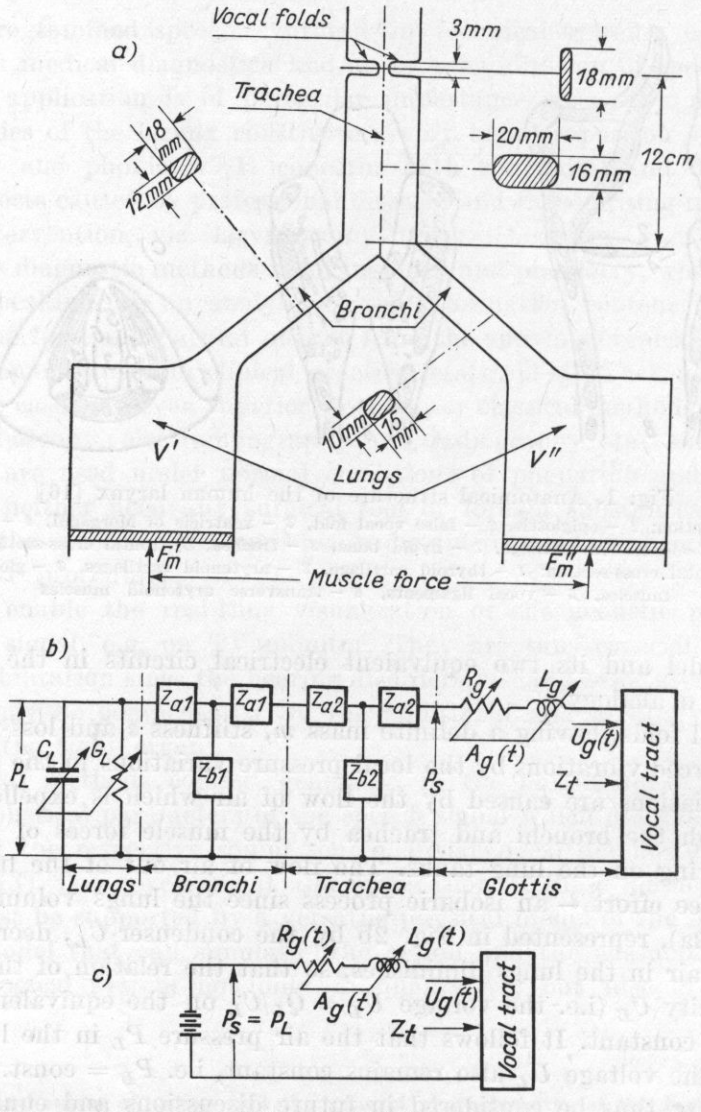

Fig. 2. Simplified physical model of the subglottal part of the human respiratory system (a) and its equivalent electrical circuits (b) (c)

of the vocal tract cavities. This resonances depend on the momentary geometrical configuration of the tract described by the tract's shape function $A_t(x)$.

In view of the relatively large cross-sectional areas (ca. 400 mm²) and small lengths (12 ÷ 15 cm) of the bronchial and tracheal tubes, represented in Fig. 2b in the form of the cascade connection of the four-poles T_1 and T_2, their longitudinal acoustic impedances are small and the corresponding pressure drops may be disregarded. Consequently, the subglottal pressure P_s is equal to the pressure P_L in the lungs, i.e. $P_s \approx P_L = \text{const}$. The total pressure drop

P_s appears across the glottis impedance Z_g and is transformed into the kinetic energy of the air flow, which is expressed in terms of the volume velocity U_g of the larynx pulses $U_g(t)$. This motivates the final simplification of the equivalent circuit in Fig. 2b to the form shown in Fig. 2c.

2.2 *Acoustic impedance of the glottis.* In Fig. 3 the glottis orifice is represented in the form of a parallelepiped slit whose geometrical dimensions correspond to the average anatomical glottis dimensions of an adult male. The effective glottis area $A_g(t) = lw(t)$ is a function of the width $w(t)$ which varies quasi-periodically as the vocal folds vibrate. In spite of such an extreme simpli-

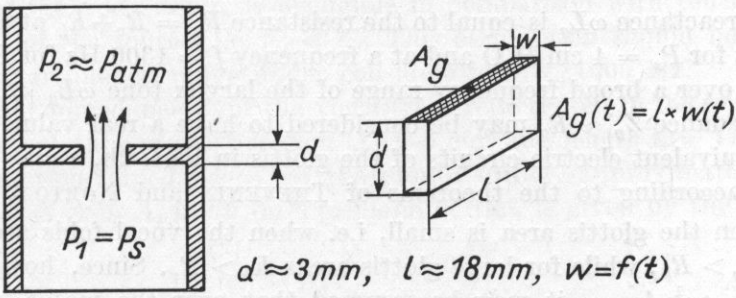

Fig. 3. Simplified physical model of the glottis

fication for the glottis' model, its acoustic impedance $Z_g = R_g + j\omega L_g$ cannot be expressed analytically by the well known formula valid for a narrow slit, as has been done in the general theory of acoustic elements and circuits (cf. e.g. [17]). The pioneers of the larynx source theory, WEGEL [15] and van den BERG et al. [1], proved that the real component R_g of the glottis impedance is the sum of two components,

$$R_g = R_v + R_k = 12\mu dl^2 A_g(t)^{-3} + 0.44\varrho A_g(t)^{-2}\,|U_g(t)|, \tag{1}$$

where $R_v \doteq A_g(t)^{-3}$ is the classical viscous loss resistance of the medium with dynamical viscosity coefficient μ, flowing through a slit of effective area $A_g(t)$, length l and depth d, $R_k \doteq A_g(t)^{-2}\,|U_g(t)|$ is the kinetic resistance referred to the process of transforming the pressure drop P_s in the glottis into kinetic energy of medium flow, according to the formula

$$P_s = \tfrac{1}{2}\varrho u^2 = \tfrac{1}{2}\varrho (U_g/A_g)^2,$$

in which u denotes the particle velocity, U the volume flow velocity and ϱ is the density of the medium.

The previous model investigations have proved that formula (1) is valid for a broad range of flow parameters: $P_s \leqslant 64$ cm H_2O, $0.1 \leqslant w(t) \leqslant 2$ mm, $|U_g| \leqslant 2000$ cm^3/s.

The reactance $j\omega L_g$ is the classical inertia of the air vibrating in the glottis and, ignoring edge-effects at the inlet and outlet of the orifice, may be expressed by the formula

$$j\omega L_g = j\omega \varrho d A_g(t)^{-1}, \tag{2}$$

where ϱ is the air density, d the depth of the slit, and $A_g(t)$ is its effective area perpendicular to the direction of flow.

Having calculated the numerical values of the components R_v, R_k and ωL_g of the glottis impedance $Z_g = (R_v + R_k) + j\omega L_g$ according to formulae (1) and (2), one can draw the following conclusions which are of use in the design of the larynx-source model:

(a) The reactance ωL_g is equal to the resistance $R_g = R_v + R_k$ at a frequency $f = 700$ Hz for $P_s = 4$ cm H_2O and at a frequency $f = 1300$ Hz for $P_s = 16$ cm H_2O. Thus over a broad frequency range of the larynx tone $\omega L_g \ll R_g$ and the glottis impedance $Z_g \approx R_g$ may be considered to have a real value. It follows that the equivalent electric circuits of the glottis in Figs. 2b, c may be further simplified according to the theorems of THEVENIN and NORTON.

(b) When the glottis area is small, i.e. when the vocal folds are near one another, $R_v > R_k$, while for large glottis areas $R_k > R_v$. Since, however, $R_v \approx R_k$ at $A_g \approx \frac{1}{5} A_{g\max}$, it may be assumed that over the major part of the vibration cycle the glottis resistance is determined by its kinetic component and, consequently, $R_g \approx R_k$.

(c) The time constant $\tau = L_g/R_g$ is always smaller than both L_g/R_v and L_g/R_k and does not exceed the value $\tau_{\max} = 0.25$ ms (Fig. 4). The time constant $\tau = L_g/R_g$ is thus one order of magnitude smaller than the shortest period

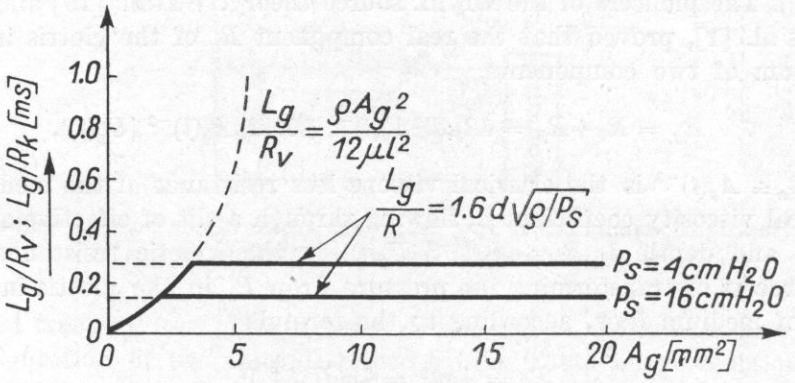

Fig. 4. Time constant L_g/R_v and L_g/R_k of the larynx oscillator as functions of the area A_g of the glottis orifice [4]

of vocal fold vibration $T_{\min} = 2.5$ ms, which corresponds to the highest larynx tone frequency of male voices $F_0 \approx 400$ Hz. It follows that the flow of air through the glottis, i.e. the volume velocity function $U_g(t)$, may be deter-

mined from the formula

$$U_g(t) = P_s/R_g(t) \approx P_s/R_k(t), \tag{3}$$

which is valid for steady flow only.

Under average anatomical conditions of an adult male ($A_{gav} \approx 5$ mm^2), at medium voice effort ($P_s \approx 10$ cm H_2O) and over the frequency range $f \ll 5000$ Hz, the acoustic impedance of the glottis $Z_g \approx [90 + j\omega 7 \times 10^{-3}]10^5$ MKS acoustic ohms, and its modulus $|Z_g| \approx 100 \cdot 10^5$ MKS acoustic ohms.

2.3. *Acoustic input impedance of the vocal tract.* Formula (3), which determines the volume velocity $U_g(t)$ of the glottal source, was a priori based on the assumption that the load impedance of the source, i.e. the input impedance Z_t of the vocal tract, is negligible in comparison with the internal impedance Z_g of the source, i.e. $Z_t \ll Z_g$. This assumption should now be justified for the frequency range under consideration $f \leqslant 1000$ Hz.

The input impedance Z_t of the vocal tract represented in the form of a lossless cylindrical tube of cross-section $A_t = 5$ cm^2 and length $l_t = 17$ cm, loaded by the radiation impedance Z_r of the mouth orifice, approximated by a circular piston of area A_t in an infinite plane baffle[1], is given by the formula

$$Z_t = Z_0 \frac{Z_r + Z_0 \tan(\beta l_t)}{Z_0 + Z_r \tan(\beta l_t)}, \tag{4}$$

in which $Z_0 = \varrho c/A_t$ is the characteristic impedance of the tube, $\beta = \omega/c = 2\pi/\lambda$ is the propagation constant, Z_r is the radiation impedance of a circular piston of radius r and $A_t = \pi r^2$ is the area.

Hence

$$Z_r \approx \frac{\varrho c}{A_t}\left[\frac{(\beta r)^2}{2} + j\frac{8}{3\pi}(\beta r)\right]. \tag{5}$$

In model investigations the radiation impedance Z_r (5) may be represented in the form of the parallel connection of the radiation resistance R_R,

$$R_R = 128/9\pi^2\left(\frac{\varrho c}{A_t}\right), \tag{5a}$$

and the inductance L_R,

$$L_R = 8r/3\pi c\left(\frac{\varrho c}{A_t}\right), \tag{5b}$$

which simulates the mass of the co-vibrating medium (cf. e.g. [4], p. 33).

It may be proved [10] that, according to the general theory of acoustic wave-guides, the function $Z_t(f)$ (4) depends strongly on frequency, and its

[1] This is the commonly accepted physical simulation of articulation conditions in the case of the neutral mouth vowel ə.

maximum values $Z_{t\max}$, which correspond to $\lambda/4$ — resonances of the vocal tract, that is to odd multiples of 500 Hz, decrease asymptotically with increasing frequency. The decreasing $Z_{t\max}$ values are comparable with the acoustic impedance Z_g of the glottis only in the vicinity of the first formant $F_1 \approx 500$ Hz ($Z_{t\max F1} \approx 86 \times 10^5 \times e^{-j77^\circ}$ MKS acoustic ohms) and of the second formant $F_2 \approx 1500$ Hz ($Z_{t\max F2} \approx 24 \times 10^5 \times e^{-j56^\circ}$ MKS acoustic ohms), approaching a limiting value equal to the characteristic impedance of the vocal tract itself $Z_0 = 8.5 \times 10^5$ MKS acoustic ohms.

It thus follows that the a priori condition $Z_t \ll Z_g$ is fulfilled over the whole of the frequency range under consideration. The larynx source may thus be treated as a constant current source since it delivers a constant volume velocity, independent of the momentary configuration of the vocal tract which affects the value and ahape of the flow function in the vicinity of the first and second formants only. This influence may, in fact, be observed in experimental investigations.

2.4. *Time and frequency characteristics of the larynx source.* Typical examples of the laryngeal pulses are shown in Fig. 5. Each pulse is represented by a single period of the glottis area function $A_g(t)$ during phonation (continuous line) and by a period of the flow function, i.e. the volume velocity $U_g(t)$ in the glottis (broken line) [2]. Both functions correspond to the articulation of the neutral vowel Э in various conditions of phonation ($P_s = 4 \div 24$ cm H_2O, $F_0 = 111 \div 250$ Hz). In view of the previously discussed independence of the source characteristics and the vocal tract configuration, the laryngeal pulses in Fig. 5 can also be considered to be representative for all other voiced sounds. The comparison of the functions $U_g(t)$ and $A_g(t)$ suggests the following conclusions:

(a) Both functions are triangular — a general and common feature of laryngeal pulses. The slopes of the flow pulses $U_g(t)$ are, however, somewhat steeper than those of the area pulses $A_g(t)$. This fact might be indirectly deduced from formula (3) in which the resistance $R_g(t)$, determined by the expression (1), is inversely proportional to the second or third power of $A_g(t)$. The steepness of the flow function pulses $U_g(t)$ results in somewhat higher levels of spectral components in the upper frequency range, as compared with those of the area function $A_g(t)$.

(b) An increase of the vocal effort or phonation intensity, which corresponds to higher values of the subglottal pressure P_s, results in a shortening of the open period τ_0 of the glottis. This effect may be expressed analytically by the decrease in the duty factor $\vartheta = \tau_0/T_0$, from $\vartheta \approx 1$ at $P_s = 4$ cm H_2O to $\vartheta = 0.5 \div 0.6$ at $P_s = 24$ cm H_2O, provided that the fundamental frequency F_0 of the larynx tone is kept constant.

The spectral characteristics of the larynx source function $U_g(t)$ or $A_g(t)$ are normally considered in the complex frequency plane $s = \sigma + j\omega$ using the

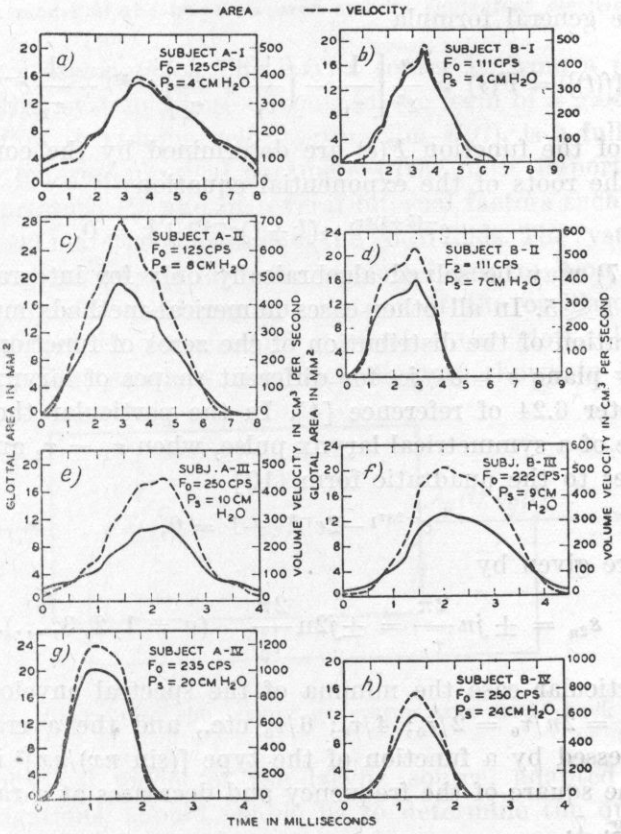

Fig. 5. Typical examples of the larynx pulses at various fundamental frequencies F_0 and different vocal efforts P_s [2]. The glottis area function $A_g(t)$ — continuous line. The flow function $U_g(t)$ — broken line

Laplace transformation. In Fig. 6 an approximation of the larynx pulse is shown in the form of a triangle of amplitude a, rise time τ_1, decay time $\tau_2 = k\tau_1$, length $\tau_0 = \tau_1 + \tau_2 = (k+1)\tau_1$ and duty factor $\vartheta = \tau_0/T_0$, where $T_0 = 1/F_0$ is the larynx tone period. The Laplace transformation of such a pulse may be ex-

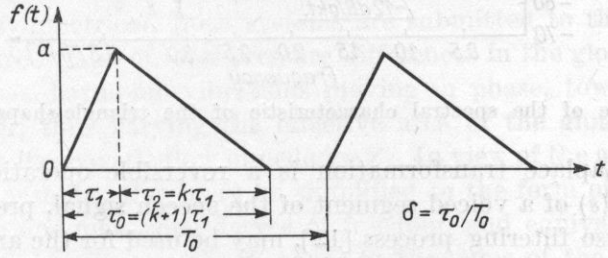

Fig. 6. Approximation of the larynx pulse in the form of a triangle

pressed by the general formula

$$\mathcal{L}\{f(t)\} = F(s) = \frac{a}{s^2}\left[\frac{1}{\tau_1} - \left(\frac{1}{\tau_1}+\frac{1}{\tau_2}\right)e^{-s\tau_1} + \frac{1}{\tau_2}e^{-s\tau_0}\right]. \tag{6}$$

The zeros of the function $F(s)$ are determined by the complex values of s, which are the roots of the exponential equation

$$e^{-(k+1)s\tau_1} - (k+1)e^{-s\tau_1} + k = 0. \tag{7}$$

Equation (7) may be solved algebraically only for integral values of k in the range $1 \leqslant k \leqslant 5$. In all other cases numerical methods must be used. Detailed consideration of the distribution of the zeros of function (6) in the complex frequency plane $s = \sigma + j\omega$ for different shapes of larynx pulses may be found in chapter 6.24 of reference [4]. In the particular though frequently-occurring case of a symmetrical larynx pulse, when $\tau_1 = \tau_2$ and $k = 1$, equation (7) reduces to the quadratic form [10]

$$e^{-2s\tau_1} - 2e^{-s\tau_1} + 1 = 0, \tag{8}$$

whose roots are given by

$$s_{2n} = \pm jn\frac{2\pi}{\tau_1} = \pm j2n\frac{2\pi}{\tau_0} \qquad (n = 1, 2, 3, \ldots). \tag{9}$$

In this particular case the minima of the spectral envelope occur at the frequencies $f_{2n} = 2n/\tau_0 = 2/\tau_0;\ 4/\tau_0;\ 6/\tau_0$ etc., and the average level of the envelope, expressed by a function of the type $[(\sin nx)/nx]^2$ is inversely proportional to the square of the frequency and decreases at a rate of 12 dB per octave, see Fig. 7.

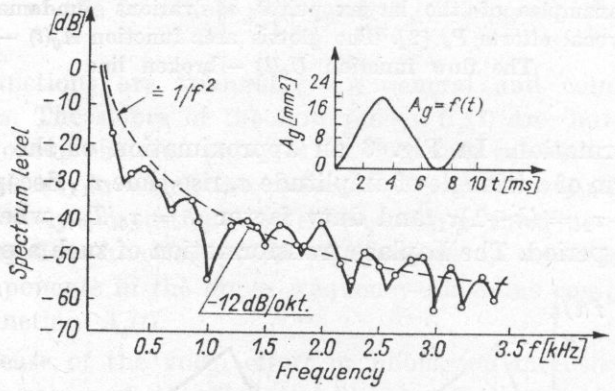

Fig. 7. Example of the spectral characteristic of the triangle-shaped larynx pulse

Since the Laplace transformation is a reversible operation, the spectral characteristic $F(s)$ of a voiced segment of the speech signal, previously submitted to the inverse filtering process [12], may be used for the analytical evaluation of the shape of the larynx pulses $U_g(t) = \mathcal{L}^{-1}\{U(s)\}$. This fact is very important in computer-aided phoniatric diagnostics.

3. Mechanical model of the larynx source and its equivalent electrical circuit

3.1. *Preliminary assumptions.* The larynx source is, from a physical point of view, a generating system whose output, in the form of a glottis area function $A_g(t)$ and a flow or volume velocity function $U_g(t)$, is a fully determined function of a few exterior physical parameters (the most important of which is the subglottal pressure P_s) and of several internal factors such as the structural parameters and material constants of the vocal folds. The system as a whole is subjected to feed-back in the form of the glottal area function $A_g(t)$ and the flow function $U_g(t)$, which – being the output of the oscillator – influence its internal parameters, i.e. those which determine the glottis impedance Z_g. These relations are illustrated by the block diagram shown in Fig. 8.

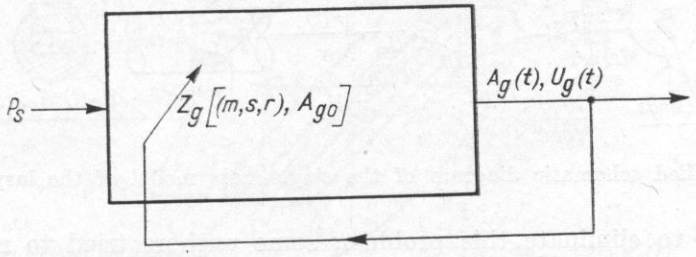

Fig. 8. Block diagram of the larynx generator as a feed – back system

A versatile physical model of the larynx source, adapted to acoustical diagnostic investigations, should enable us to determine the quantitative relations between the internal parameters of the source itself and its output $U_g(t)$ expressed in terms of directly measurable acoustic quantities, such as the acoustic pressure $p(t)$ of the sound wave in front of the patient's mouth.

3.2. *Mechanical model of the larynx source.* In the majority of papers concerning the larynx source, the vocal folds are presented in the form of a simple mechanical vibrating system with lumped constants, which consists of two indeformable masses m', m'', springs of stiffness s', s'' and viscous loss resistances r', r''. As a rule, both vibrating systems (m', s', r') and (m'', s'', r''), which simulate the left and the right vocal fold, respectively, are considered to be mutually symmetrical. Both systems are submitted to the action of the subglottal pressure P_s and of local pressure differences in the glottis. As a result they perform quasi-harmonic vibrations moving in phase, towards and away from one another, thus varying the effective area of the glottis orifice $A_g(t)$ and consequently its acoustic flow impedance Z_g. In view of the above symmetry of the vibrating systems, they may be simplified to the form of a single vibrating system with one mass, one degree of freedom, and equivalent parameters $m = m' + m''$, $s = s' + s''$, $r = r' + r''$ equal to the sums of the respective partial constants. The detailed analysis of such a single-mass model may be found

in [4, 5]. The simplified scheme of the single-mass model of the larynx source is shown in Fig. 9, according to [4].

This model, though relatively simple and thus convenient for analytical interpretation, proved, however, to be unsatisfactory in phoniatric diagnostics. The reason for this was that it did not take into account an essential physiological factor connected with the anatomical structure and the cinematics of the vocal folds. This feature is the deformability of the vocal folds resulting in an asymmetry of vibration and in phase shifts between the displacements of their lower and upper parts or edges in quasi-harmonic motion.

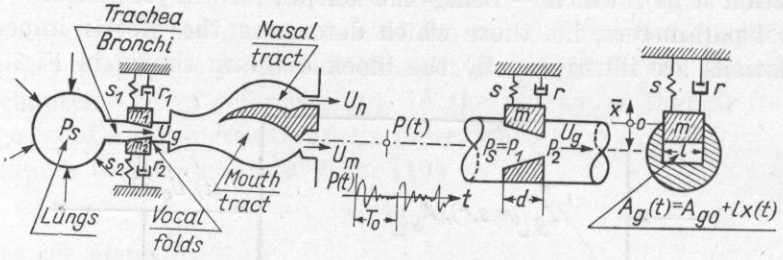

Fig. 9. Simplified schematic diagram of the single-mass model of the larynx source [4]

In order to eliminate this problem, some authors tried to represent the vocal folds as mechanical systems with continuously distributed constants, that is consisting of an infinite number of elementary masses, springs and loss resistances. Such a proposition [6], although theoretically based and quite possible in practice, due to the almost unlimited facilities offered by computing techniques, is neither necessary nor convenient in medical diagnostics, since the fundamental physiological and pathological features of the human larynx source may be simulated with sufficient accuracy in the two-mass model with lumped constants, proposed by ISHIZAKA and MATSUIDARA [7], presented by FLANAGAN [3] to the 7th ICA in Budapest and described in [9].

3.3. *The two-mass model of the larynx source.* Figure 10 presents a simplified scheme of the two-mass model in two cross-sectional planes: the vertical X-Y (a) and the horizontal X-Z (b), and its situation in the X-Y-Z axis system (c). The essential characteristic features of the two-mass model are the following:

(a) The depth d of the glottis slit is divided into two segments d_1 and d_2 ($d = d_1+d_2$), which correspond to the masses m_1 and m_2 representing the lower and the upper parts of the vocal fold, respectively. The areas of the glottis orifice in the segments d_1 and d_2 are given by the expressions

$$A_{g1} = A_{g01}+2x_1(t)l_g, \tag{10a}$$

$$A_{g2} = A_{g02}+2x_2(t)l_g, \tag{10b}$$

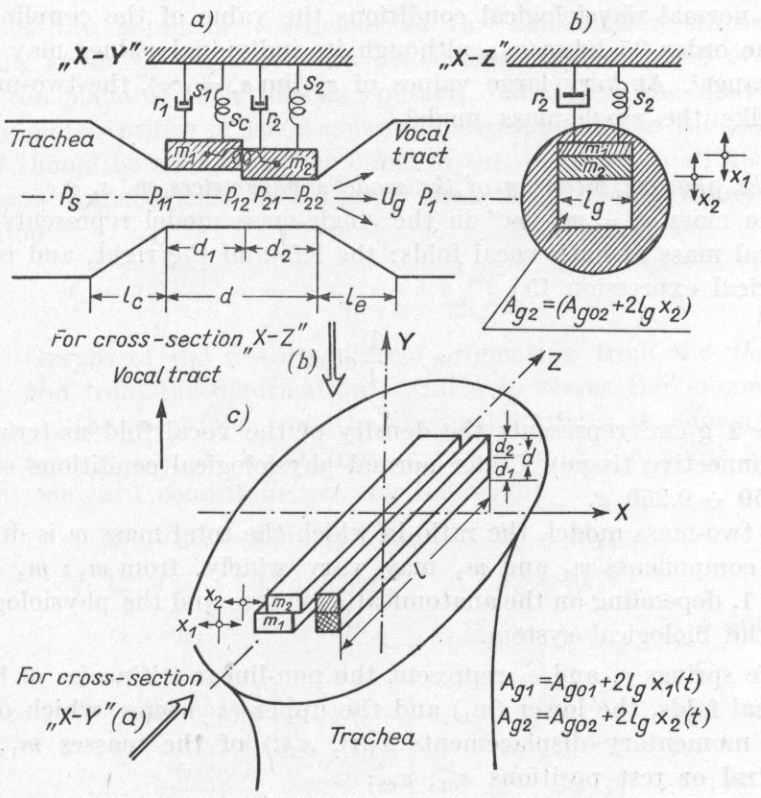

Fig. 10. Simplified schematic diagram of the two-mass model of the larynx source [9] a) horizontal cross-section X-Y, (b) vertical cross-section X-Z, (c) approximate situation of the model in the orthogonal system of space coordinates X-Y-Z

where A_{g01}, A_{g02} are the neutral or rest areas of the glottis orifice of the segments d_1 and d_2 corresponding to the glottis inlet and outlet, respectively; $x_1(t)$, $x_2(t)$ are the momentary displacements of the masses m_1 and m_2, respectively, from the neutral or rest positions.

(b) The masses m_1 and m_2 are mutually coupled by the spring s_c which represents the bending stiffness of the vocal folds in the vertical plane X-Y parallel to the direction of vibration. The coupling stiffness s_c is, in fact, a non-linear parameter which, however, may be linearized without any essential influence on the accuracy of the model. The restoring force f_c originating from the coupling stiffness s_c is given by the expression

$$f_c = 2s_c(x_1-x_2)^3(d_1+d_2)^{-2}, \tag{11a}$$

which, provided the system is linear, may be rewritten in the following simplified form:

$$f_c \approx s_c(x_1-x_2). \tag{11b}$$

Under normal physiological conditions the value of the coupling stiffness s_c is of the order 25 kdyn/cm, although its individual values may vary over a broad range[2]. At very large values of s_c ($\lim s_c = \infty$), the two-mass model behaves like the single-mass model.

3.4. *The physical meaning of the model's parameters m, s, r.*

(a) The mass $m = m' + m''$ in the single-mass model represents the equivalent total mass of both vocal folds: the left and the right, and is given by the empirical expression [5]

$$m = \frac{1}{4}\sigma l_g^2 d, \tag{12}$$

where $\sigma \approx 1$ g/cm^3 represents the density of the vocal fold material (muscular and connective tissue). Under normal physiological conditions m is of the order $0.150 \div 0.250$ g.

In the two-mass model, the ratio in which the total mass m is divided into its partial components m_1 and m_2 may vary widely, from $m_1 : m_2 = d_1 : d =$ 1 : 1 to 5 : 1, depending on the anatomical structure and the physiological constants of the biological system.

(b) The springs s_1 and s_2 represent the non-linear stiffnesses of both parts of the vocal folds, the lower (m_1) and the upper (m_2) ones, which oppose:

– the momentary displacements $x_1(t)$, $x_2(t)$ of the masses m_1, m_2 from their neutral or rest positions x_{01}, x_{02};

– the viscoelastic deformations of the vocal folds in the closing phase, when the opposite folds contact with one another, but their motion does not stop suddenly; the corresponding masses m' and m'' move slightly towards one another, being submitted to an instantaneous and reversible deformation.

The restoring force f_{sj} which originates from the stiffness s_j ($j = 1, 2$) is thus the sum of two components

$$f_{sj} = f_{kj} + f_{hj} \quad (j = 1, 2). \tag{13}$$

The first component f_{kj} denotes the restoring force due to the displacement stiffness k_j and may be expressed by the formula

$$f_{kj} = k_j x_j (1 + \eta_{kj} x_j^2) \quad (j = 1, 2), \tag{14}$$

where η_{kj} is the non-linear coefficient of the displacement stiffness k_j.

The second component f_{hj} denotes the restoring force due to the deformation stiffness h_j and may by expressed by the formula

$$f_{hj} = h_j (x_j - x_{0j})[1 + \eta_{hj}(x_j - x_{0j})^2] \quad (j = 1, 2;\ x_j \geqslant x_{0j}), \tag{15}$$

[2] The numerical values of the equivalent mechanical constants of the biological larynx source system are quoted from [8].

where η_{hj} is the nonlinear coefficient of the deformation stiffness h_j, $x_{0j} = -A_{g0j}/2l_g$ is the distance between the neutral or rest plane of the vocal folds and the plane of their mutual contact, and A_{g0j} is the neutral or rest area of the glottis orifice of the segment d_j corresponding to the mass m_j ($j = 1, 2$). It should be noted that the effect of the deformation stiffness appears only for large displacements x_j, i.e. larger than the threshold values x_{0j}, when the condition

$$x_j \geqslant x_{0j} = -\frac{A_{g0j}}{2l_g} \tag{16}$$

is fulfilled. Graphs of the restoring forces originating from the displacement stiffness k_j and from the deformation stiffness h_j versus the momentary displacement x_j of the vocal folds from their neutral positions are shown in Fig. 11.

The average values of the stiffness parameters of the vocal folds under normal physiological conditions are the following:

$$k_1 = 50 \div 100 \text{ kdyn/cm}, \qquad h_1 \approx 3k_1,$$

$$k_2 = 5 \div 50 \text{ kdyn/cm}, \qquad h_2 \approx 3k_2,$$

$$\eta_{k1},\ \eta_{k2} = 50 \div 100, \qquad \eta_{h1},\ \eta_{h2} = 250 \div 500.$$

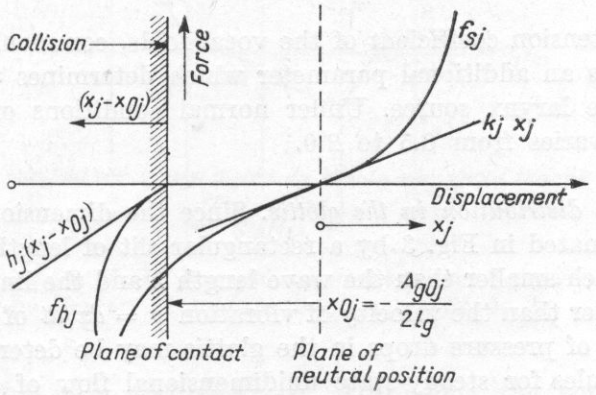

Fig. 11. Restoring forces originating from the displacement stiffness k_j and deformation stiffness h_j as functions of the momentary displacements x_j of the vocal folds from their rest positions

(c) The loss resistance r is attributed to:

– the viscous losses in the material, i.e. the muscular and connective tissue of the vocal folds,

– the mutual adhesion of the vocal folds contacting one another in the closing phase, when they move together and away from one another.

The influence of the loss resistance is an increase in the attenuation or damping coefficients ξ_1 and ξ_2 expressed by the formulae

$$\xi_1 = r_1/2\sqrt{m_1 k_1}, \qquad \xi_2 = r_2/2\sqrt{m_2 k_2}, \tag{17a, b}$$

in which k_1, k_2 are the linear coefficients of the displacement stiffness, cf. equation (14).

The average values of the damping coefficients ξ_1 and ξ_2 under normal physiological conditions are as follows:

— in the closing phase of the glottis: $\xi_1 \approx 0.1$, $\xi_2 \approx 0.6$;

— in the opening phase of the glottis: $\xi_1 \approx 1.1$, $\xi_2 \approx 1.6$.

(d) The tension coefficient Q of the vocal folds. The mass and stiffness parameters of the vocal folds determine the natural frequency f_0 of their oscillations, expressed by the formula

$$f_0 = \frac{1}{2\pi}\sqrt{\frac{s}{m}}. \tag{18a}$$

Under real conditions of phonation and articulation, due to the contraction of the vocalis muscles the vocal folds are shortened or elongated and their tension varies to a limited extent. Their mass m and stiffness s also vary and the frequency of oscillations changes from the value f_0 (18a) to the value f_0' given by the expression

$$f_0' = \frac{1}{2\pi}\sqrt{\frac{sQ}{m/Q}} = \frac{Q}{2\pi}\sqrt{\frac{s}{m}} = Qf_0, \tag{18b}$$

where Q is the tension coefficient of the vocal folds, commonly used in model investigations as an additional parameter which determines the real physical constants of the larynx source. Under normal conditions of phonation and articulation Q varies from 0.5 to 2.0.

3.5. *Pressure distribution in the glottis.* Since the dimensions of the glottal orifice, approximated in Fig. 3 by a rectangular slit of length l, width w and depth d, are much smaller than the wave length λ and the linear flow velocity u_g is much smaller than the velocity of vibration $v = dx/dt$ of the vocal fo ds, the distribution of pressure drops in the glottis may be determined according to the general rules for steady-state unidimensional flow of air along the Y axis, (see Fig. 10). The scheme of the longitudinal cross-section of the glottis model and the corresponding pressure drops ΔP along the flow axis are shown in Fig. 12a and 12b, respectively. The pressure drops are determined by the expressions (19) ÷ (23):

$$P_s - P_{11} = 0.69\varrho(U_g^2 A_{g1}^{-2}) + \int_0^{l_c} \frac{\varrho}{A_c(x)}\,dx\,\frac{dU_g}{dt}, \tag{19}$$

$$P_{11} - P_{12} = 12\mu d_1 l_g^2 A_{g1}^{-3} U_g + \frac{\varrho d_1}{A_{g1}}\,\frac{dU_g}{dt}, \tag{20}$$

$$P_{12} - P_{21} = \frac{\varrho}{2}\,U_g^2(A_{g2}^{-2} - A_{g1}^{-2}), \tag{21}$$

$$P_{21}-P_{22} = 12\mu d_2 l_g^2 A_{g2}^{-3} U_g + \frac{\varrho d_2}{A_{g2}} \frac{dU_g}{dt}, \tag{22}$$

$$P_{22}-P_1 = -\varrho U_g^2 A_{g2}^{-2} \frac{A_{g2}}{A_t}\left(1-\frac{A_{g2}}{A_t}\right). \tag{23}$$

Formulae (19) - (23) are based on the following assumptions (see Fig. 12):

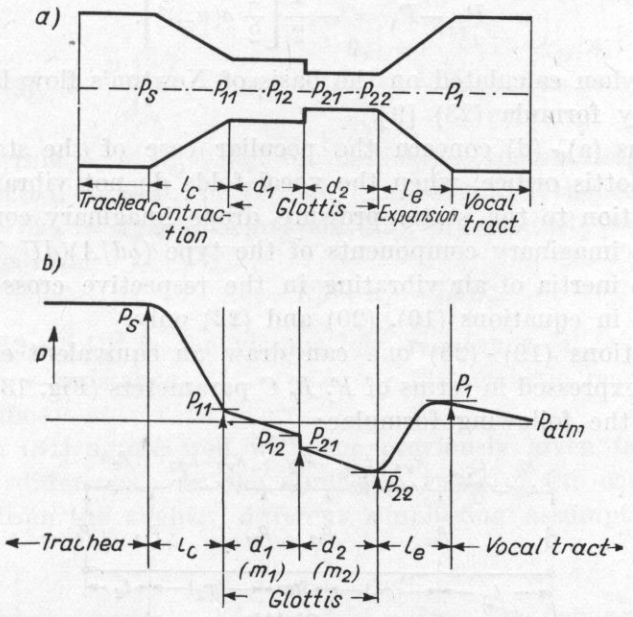

Fig. 12. Schematic diagram of the longitudinal cross-section of the glottis model (a) and the diagram of pressure drops in the glottis (b)

(a) The pressure drop $\Delta P_{lc} = P_s - P_{11}$ (19) along the constriction l_c of the trachea at the glottis inlet is equal to the Bernoulli pressure increased by an empirical coefficient $k \approx 0.37$ which expresses the effect of the constriction [1], so that, finally,

$$\Delta P_{lc} \approx 1.37 \frac{\varrho}{2} (u_{g1})^2.$$

(b) The pressure drops $\Delta P_{d1} = P_{11} - P_{12}$ (20) and $\Delta P_{d2} = P_{21} - P_{22}$ (22) along the segments d_1 and d_2, respectively, originate from the viscous loss resistances R_{v1} and R_{v2} determined by the general formula (1).

(c) The pressure drop $\Delta P_{d1/d2} = P_{12} - P_{21}$ (21) at the abrupt change of the glottis cross-sectional area is equivalent to the difference of the kinetic energy

densities in the cross-sections A_{g1} and A_{g2}, provided that the air flow in the glottis is continuous: $U_g = \text{const}$. Hence

$$P_{12} - P_{21} = \frac{1}{2} \varrho U_g^2 (A_{g2}^{-2} - A_{g1}^{-2}),$$

since $u_{g1}^2 = U_g^2 A_{g1}^{-2}$ and $u_{g2}^2 = U_g^2 A_{g2}^{-2}$.

(d) The pressure drop $\Delta P_{l_e} = P_{22} - P_1 \approx P_{22} - P_{\text{atm}}$ has a negative value; according to [1]

$$P_{22} - P_1 = -\frac{1}{2}\left[\frac{1}{2} \varrho (u_{g2})^2\right].$$

However, when calculated on the basis of Newton's flow laws, it has the value given by formula (23) [9].

Assumptions (a) - (d) concern the peculiar case of the static flow of air through the glottis orifice, when the vocal folds do not vibrate. In dynamic states of vibration to the static pressure drops imaginary components must be added. The imaginary components of the type $(\varrho d/A)(dU_g/dt)$, which are referred to the inertia of air vibrating in the respective cross-sections of the glottis, appear in equations (19), (20) and (22) only.

Using equations (19) - (23) one can draw an equivalent electrical circuit of the glottis, expressed in terms of R, L, C parameters (Fig. 13), whose values are given by the following formulae:

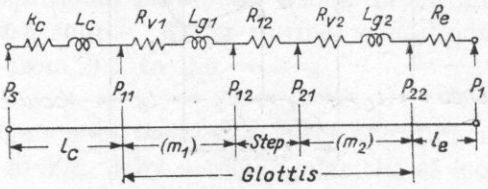

Fig. 13. Equivalent electrical circuit of the glottis

$$R_c = 0.69 \varrho A_{g1}^{-2} |U_g|, \tag{24}$$

$$L_c = \varrho \int_0^{l_c} \frac{dx}{A_c(x)}, \tag{25}$$

$$R_{v1} = 12 \mu l_g^2 d_1 A_{g1}^{-3}, \tag{26}$$

$$L_{g1} = \varrho d_1 A_{g1}^{-1}, \tag{27}$$

$$R_{v2} = 12 \mu l_g^2 d_2 A_{g2}^{-3}, \tag{28}$$

$$L_{g2} = \varrho d_2 A_{g2}^{-1}, \tag{29}$$

$$R_{12} = \frac{1}{2} \varrho (A_{g2}^{-2} - A_{g1}^{-2}) |U_g|, \tag{30}$$

$$R_e = -\varrho \frac{|U_g|}{A_{g2} A_t} \left(1 - \frac{A_{g2}}{A_t}\right). \tag{31}$$

The acoustic impedance Z_g of the glottis in the two-mass model, determined on the basis of the equivalent circuit in Fig. 13, may be expressed as

$$Z_g = \frac{\varrho}{2}|U_g|\left[\frac{0.37}{A_{g1}^2} + \frac{1-2\dfrac{A_{g2}}{A_t}\left(1-\dfrac{A_{g2}}{A_t}\right)}{A_{g2}^2}\right] + (R_{v1}+R_{v2}) + j\omega(L_{g1}+L_{g2}+L_c)$$

$$= (R_{k1}+R_{k2})|U_g| + (R_{v1}+R_{v2}) + j\omega(L_{g1}+L_{g2}+L_c), \tag{32}$$

where

$$R_{k1} = \frac{0.19\varrho}{A_{g1}^2}, \qquad R_{k2} = \varrho\frac{0.5-\dfrac{A_{g2}}{A_t}(1-A_{g2}/A_t)}{A_{g2}^2}. \tag{33a,b}$$

Since as a rule $L_c \ll L_{g1}+L_{g2}$, the inductance representing the inertia L_c may be neglected, $L_c \approx 0$. In the single-mass model the coupling stiffness $s_c = \infty$, $A_{g1} = A_{g2} = A_g$ and expression (32), provided $A_g \gg A_t$, may be rewritten in the form

$$Z_g' = R_v' + R_k' + j\omega L_g', \tag{34}$$

where $R_v' = 12\mu d l_g^2 A_g^{-3}$ is the viscous loss resistance, $R_k' = 0.69\varrho A_g^{-2}|U_g|$ — the kinetic flow resistance, $L_g' = \varrho d A_g^{-1}$ — the acoustic mass of the air in the glottis orifice.

Expression (34) agrees well with the previously given formulae (1) and (2). The only difference — in the numerical value of the constant factor in R_k' — results from the slightly different simplifying assumptions in the case considered.

3.6. *The driving forces in the vocal fold system.* The driving forces, denoted as F_1 and F_2, originate from the pressures P_{m1} and P_{m2} which act on the effective side areas of the vocal folds equal to $(l_g d_1)$ and $(l_g d_2)$, respectively. It is assumed that P_{m1} and P_{m2} are equal to the arithmetic means of the pressures (P_{11}, P_{12}) and (P_{21}, P_{22}) respectively, thus

$$P_{m1} = \frac{1}{2}(P_{11}+P_{12}), \tag{35}$$

$$P_{m2} = \frac{1}{2}(P_{21}+P_{22}). \tag{36}$$

Using equations (19)-(23), one can write

$$P_{m1} = \frac{1}{2}(P_{11}+P_{12}) = P_s - R_c U_g - \frac{1}{2}\left(R_{v1}U_g + L_{g1}\frac{dU_g}{dt}\right), \tag{35a}$$

$$P_{m2} = \frac{1}{2}(P_{21}+P_{22}) = P_{m1} - R_{12}U_g - \frac{1}{2}\left[(R_{v1}+R_{v2})U_g + (L_{g1}+L_{g2})\frac{dU_g}{dt}\right], \tag{36a}$$

and finally obtain

$$F_1 = P_{m1}(l_g d_1), \tag{37a}$$

$$F_2 = P_{m2}(l_g d_2). \tag{37b}$$

4. Electrical model of the larynx source and its mathematical description

4.1. *Electrical equivalent circuit of the model.* Having introduced the simplifying assumptions previously discussed which consist in:

(a) disregarding the acoustic impedances of the bronchi and trachea,

(b) representing the energy source, that is the lungs, by a d.c. voltage source with electromotive force $P_s \approx P_L$ and zero internal impedance,

(c) expressing the glottis impedance Z_g in the form given by equation (32), one may draw the electric equivalent circuit of the speech organ in vowel articulation as shown in Fig. 14. The pharynx-mouth vocal tract is simulated by the cascade connection of n symmetrical T-type four-poles, each of which represents an elementary section of the vocal tract approximated in the form of a cylindrical tube with hard walls, of cross-sectional area A_i and length l_i ($i = 1, 2, \ldots, n$). The acoustic parameters of the i-th four-pole T_i are as follows [10]:

$L_i = \varrho l_i / A_i$ — acoustic mass,

$C_i = A_i l_i / \varrho c^2$ — acoustic compliance,

$R_i = (S_i l_i / A_i^2)\sqrt{\varrho \mu \omega / 2}$ — acoustic resistance of the viscous losses at the tube walls, where ϱ is the density of air, μ — the coefficient of viscosity, S_i — the tube circumference and $\omega = 2\pi f$ — the angular frequency. The neglected losses, caused by energy absorption at the walls of the tube and by heat conduction at the walls, may be taken into account by multiplying the acoustic loss resistance R_i, calculated at the frequency $f = F_0$, by the correction factor $k = 20\text{-}25$.

In the equivalent circuit given in Fig. 14, the radiation impedance Z_r is represented in the form of the parallel connection of the inductance L_R and radiation resistance R_R, according to the expressions (5), (5a) and (5b) in section 2.3.

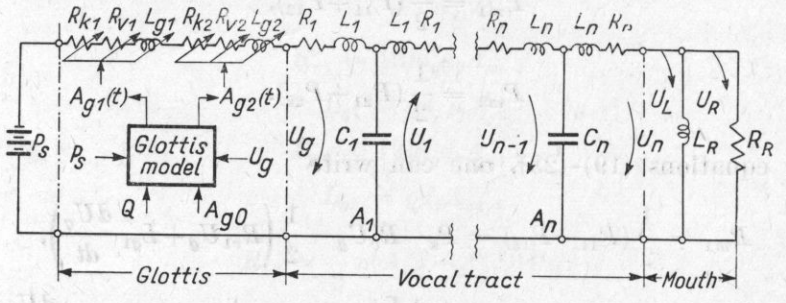

Fig. 14. Equivalent electrical circuit of the speech organ in vowel articulation

4.2. *Mathematical description of the model.* The behaviour of the electric circuit in Fig. 14 may be easily discussed by the classical methods of network analysis, e.g. by the loop-current method for $n+2$ loops, where n is the arbitrary number of elementary segments of the vocal tract. Let us for example put $n = 4$, thus simulating the vocal tract by four cylindrical segments only. In this case we obtain the set of six differential equations of motion (38)-(43):

$$(R_{k1}+R_{k2})|U_g|U_g+(R_{v1}+R_{v2})U_g+(L_{g1}+L_{g2})\frac{dU_g}{dt}+$$

$$+R_1U_g+L_1\frac{dU_g}{dt}+\frac{1}{C_1}\int_0^t(U_g-U_1)dt=P_s, \tag{38}$$

$$(R_1+R_2)U_1+(L_1+L_2)\frac{dU_1}{dt}+\frac{1}{C_2}\int_0^t(U_1-U_2)dt+\frac{1}{C_1}\int_0^t(U_1-U_g)dt=0, \tag{39}$$

$$(R_2+R_3)U_2+(L_2+L_3)\frac{dU_2}{dt}+\frac{1}{C_3}\int_0^t(U_2-U_3)dt+\frac{1}{C_2}\int_0^t(U_2-U_1)dt=0, \tag{40}$$

$$(R_3+R_4)U_3+(L_3+L_4)\frac{dU_3}{dt}+\frac{1}{C_4}\int_0^t(U_3-U_L)dt+\frac{1}{C_3}\int_0^t(U_3-U_2)dt=0, \tag{41}$$

$$R_4U_L+(L_4+L_R)\frac{dU_L}{dt}-L_R\frac{dU_R}{dt}+\frac{1}{C_4}\int_0^t(U_L-U_3)dt=0, \tag{42}$$

$$R_RU_R+L_R\frac{d}{dt}(U_R-U_L)=0. \tag{43}$$

From these equations the currents (or volume velocities U) and voltages (or acoustic pressures p) in any loop and node of the network corresponding to a particular acoustic cross-section of the vocal tract may be determined. In acoustic diagnostics of the larynx source the following quantities and the mutual relationships are the most interesting:

(a) The volume velocity U_g in the glottis orifice as the output of the larynx source in the form of the flow function $U_g(t)$.

(b) The volume velocity U_R through the radiation resistance R_R of the mouth orifice, since this quantity is functionally connected to a directly measurable diagnostic parameter of the speech signal, viz. the acoustic pressure $p(r)$ at a distance r from the mouth orifice

$$p(r)=\frac{j\omega\varrho U_R}{4\pi r}e^{-j2\pi r/\lambda}. \tag{44}$$

Relation (44) is valid in the near field of a spherical wave, when $2\pi r \leqslant \lambda$.

The coefficients R_{k1}, R_{k2}, R_{v1}, R_{v2}, L_{g1}, L_{g2} in equation (38), which also appear in expression (32) for the acoustic impedance Z_g of the glottis, are functions of the glottis areas $A_{g1}(t)$ (10a) and $A_{g2}(t)$ (10b). This fact is attributed to the feed-back in the larynx generator, previously described in section 3.1. In this connection the flow equations (38)-(43) must be complemented by the differential equations of motion of the vocal folds, simulated by the masses m_1 and m_2. The equations of motion may be written in the form

$$F_1 = m_1 \frac{d^2x_1}{dt^2} + r_1 \frac{dx_1}{dt} + s_1 x_1 + s_c(x_1 - x_2), \tag{45a}$$

$$F_2 = m_2 \frac{d^2x_2}{dt^2} + r_2 \frac{dx_2}{dt} + s_2 x_2 + s_c(x_2 - x_1), \tag{45b}$$

where F_1 and F_2 are the driving forces given by formulae (35), (36) and (37).

For the purposes of numerical calculations and computer modelling of the speech organ in various conditions of phonation and articulation, the differential equations of flow (38)-(43) and motion (45a, b) should be made discrete by substituting for the differentiation $[df(t)/dt]$ and integration $[\int f(t)dt]$ operators the corresponding incremental approximations according to the rules

$$\frac{df(t)}{dt} \approx \frac{f(t_i) - f(t_{i-1})}{t_i - t_{i-1}} = \frac{f_i - f_{i-1}}{\tau}, \tag{46a}$$

$$\int f(t)dt \approx (t_i - t_{i-1}) \sum_{i=0}^{i-1} f_i = \tau \sum_{i=0}^{i-1} f_i, \tag{46b}$$

where τ is the step of time quantization, and i is the number of the successive time segments.

The flow and motion equations must be solved by an iterative method. The volume velocities U in the different cross—sections of the vocal tract, the driving forces F_1, F_2 and the resulting displacements x_1, x_2 of the vocal folds m_1, m_2 in successive i-th time segments are determined from the values of x_1 and x_2, calculated or assumed for the preceeding, that is (i-1)-th, time segment.

5. Conclusions

The preceeding theoretical considerations indicate the applicability and usefulness of a physical model of the human larynx source in diagnostic investigations of the speech organ in both normal and pathological cases. Any anomaly of the anatomical structure of the larynx and restriction of its motive capability, resulting either from laryngeal nerve palsy or from necessary surgical intervention, may be expressed in terms of the physical parameters of the model, which at the same time result in measurable variations of the acous-

tic structure of the speech signal being analysed in the time and/or frequency domains. These relations are mutual and reversible: the analysis of the acoustic parameters of the speech signal under definite phonation and articulation conditions makes it possible to determine, when using the model and its mathematical description, the equivalent values of the physical parameters of the larynx model and hence to define and localize any anomaly of the anatomical structure or reason for a restricted motive capability of the biological system. This in turn facilitates and makes objective the process of diagnosis.

The directly measurable acoustical diagnostic signal usually used in laryngology and phoniatry is the acoustic pressure $p(t)$ of the speech wave at a particular point on the axis of symmetry of the patient's mouth, or the spectral presentation of this function obtained by a Fourier or Laplace transformation. The acoustic pressure is connected with the volume velocity U_R in the mouth orifice by the simple relation (44). The time and frequency parameters of the $U_R(t)$ function contain essential information concerning the physical and material constants of the larynx source, as well as the spectral (e.g. formant--antiformant) structure of the speech signal-which depends on the momentary geometrical configuration of the vocal tract. The latter information may, if necessary, be eliminated by the process of inverse filtering. In this way the information content of the speech signal may be limited to the larynx source characteristics only. The essential diagnostic information is contained in the volume velocity function $U_g(t)$ through the glottis, since this function is related by the flow equations (38)-(43) and the motion equations (45) with the most important physical and physiological parameters of the vocal folds and with the subglottal pressure P_s.

The physical interpretation of the larynx pathology and the description of anatomical anomalies in terms of the physical parameters of the diagnostic speech signal is the subject of further research work which is being carried out in the Speech Acoustics Laboratory, Department of Cybernetic Acoustics, IFTR[3]) – Polish Academy of Sciences, in close co-operation with the Phoniatric Centre[4]) of the Otolaryngological Clinic, Central Clinical Hospital, Medical Academy in Warsaw.

References

[1] J. W. VAN DEN BERG, J. T. ZANTEMA, P. DOORNENBAL Jr., *On the air resistance and the Bernoulli effect of the human larynx*, J. Acoust. Soc. Amer., **29**, 626-631 (1957).

[2] J. L. FLANAGAN, *Some properties of the glottal sound source*, J. Speech Hearing Res., **1**, 99-116 (1958).

[3] J. L. FLANAGAN, *Focal points in speech communication research*, Proc. of the 7th Int. Congress on Acoustics, ICA, Budapest, paper 21-G-3 (1971).

[3] Institute of Fundamental Technological Research, Warsaw, Poland.

[4] Head of the Centre: Ass. Prof. Witold Tłuchowski, M. D.

[4] J. L. FLANAGAN, *Speech analysis, synthesis and perception*, Springer-Verlag, 2nd edition, Berlin-Heidelberg-New York 1972.

[5] J. L. FLANAGAN, L. L. LANDGRAF, *Self-oscillating source for vocal-tract synthesizers*, IEEE Trans. Audio and Electroacoustics, **AU-16**, 57-64 (1968).

[6] K. ISHIZAKA, *On models of the larynx*, J. Acoust. Soc. Japan, **22**, 293-294 (1966).

[7] K. ISHIZAKA, M. MATSUIDARA, *What makes the vocal cords vibrate*, Proc. 6th Int. Congress on Acoustics, ICA, Tokyo, paper B1-3 (1968).

[8] K. ISHIZAKA, T. KANEKO, *On equivalent mechanical constants of the vocal cords*, J. Acoust. Soc. Japan, **24**, 312-313 (1968).

[9] K. ISHIZAKA, J. L. FLANAGAN, *Synthesis of voiced sounds from a two-mass model of the vocal cords*, Bell Syst. Tech. J., **51**, 1233-1268 (1972).

[10] J. KACPROWSKI, *Theoretical bases of the synthesis of Polish vowels in resonance circuits*, Speech Analysis and Synthesis, volume 1, 219-287, PWN (Polish Scientific Publishers), Warsaw 1968.

[11] J. KACPROWSKI, W. MIKIEL, A. SZEWCZYK, *Acoustical modelling of cleft-palate*, Archives of Acoustics, **1**, 2, 167-187 (1976).

[12] R. L. MILLER, *Nature of the vocal chord wave*, J. Acoust. Soc. Amer., **31**, 667-677 (1959).

[13] W. TŁUCHOWSKI, W. MIKIEL, A. NIEDŹWIECKI, A. KOMOROWSKA, *Phonospectroscopic investigations in one-sided and two-sided paralysis of laryngeal nerves*, Diary of the 29th Meeting of Polish Oto-Laryngologists, Białystok 1974, pp. 359-363 (in Polish).

[14] W. TŁUCHOWSKI, J. KACPROWSKI, W. MIKIEL, A. NIEDŹWIECKI, A. KOMOROWSKA, *Clinical phonospectroscopy – a preliminary report*, Otolaryngologia Polska, **29**, 3, 251-259 1975 (in Polish).

[15] R. L. WEGEL, *Theory of vibration of the larynx*, Bell Syst. Tech. J., **9**, 207-227 (1930).

[16] B. WIERZCHOWSKA, *Polish pronunciation*, PZWS (Polish Educational Publishers) 2nd edition, Warsaw 1971 (in Polish).

[17] Z. ŻYSZKOWSKI, *Fundamentals of electroacoustics*, WNT (Scientific and Technical Publishers), 2nd edition, Warsaw 1966 (in Polish).

Received on 26th July 1976

ARCHIVES OF ACOUSTICS
2, 1, 71-79 (1977)

VARIABILITY OF THE HEARING THRESHOLD TRACINGS IN AUTOMATIC AUDIOMETRY BEYOND THE INITIAL TRANSIENT PHASE

ANTONI JAROSZEWSKI, ANDRZEJ RAKOWSKI

Labolatory of Musical Acoustics, Academy of Music (Warszawa)

The results of measurements and the analysis of variability of the hearing threshold observed in automatic audiometry beyond the initial transient phase are given. The methods of interpretation of the threshold tracings and their adequacy with respect to various rates of the test signal level control are discussed.

1. Introduction

It is well-known that the hearing threshold level in individuals is far from being constant even if the temporary threshold shifts due to exposure to high intensity sounds is not taken into account [1, 2, 3].

Beyond the initial transient phase in the tracing, which, with regard to its presumable origin and dependency on the experimental conditions has been discussed in the previous report [10], the hearing threshold undergoes fluctuations resulting from a number of various factors. Among these factors in the earlier studies three main groups were recognized, i.e. physiological (heart action, blood pressure, body temperature, degree of fatigue etc), physical (atmospheric pressure) [4] and psychological such as short term variations of the reaction time and changes in the threshold detection criteria as well as practice and motivation in the subjects [5, 6, 8, 13, 14].

Threshold level depends also in a considerable degree on the pattern of presentation of the stimuli, particularly on the rate of signal level control and on the duration of the measurement. CORSO'S findings [5, 6] which do not reveal substantial influences of neither the rate of signal level control nor the duration of the measurement were not to the authors' knowledge confirmed in the observations by other authors. Some implications leading to the conclusion contradictory to the results reported in CORSO'S works can be inferred from the data published by HEMPSTOCK et al. [7]. According to these data, after the elapse of abt. 15 min from the beginning of the measurement, the difference in hearing thresholds for the continuous and the interrupted tone amounts to abt. 5 dB. Also from ZWISLOCKI'S et al. [14]. report it is evident that the hea-

ring threshold level, as determined by Békésy's audiometer tracings, is clearly dependent on the duration of the measurement.

In the analysis of the figured factors influence it should be remembered that the signal level taken as a hearing threshold level results from the definite statistical operation and hence depends on the convention applied. In automatic audiometers (Békésy type audiometers) this comes to the method of interpretation of the hearing threshold tracings in the attempt to determine these values of the signal level which are taken as the hearing threshold level.

In conventional clinical audiometers in which signal level is controlled manually, the rate of signal level control near the threshold is usually quite small, of the order of 0.5 — 3.0 dB/s. Also the effective duration of the measurement at the separate discrete frequencies usually does not exceede a few seconds. It should be pointed out that as an effective duration of the measurement only this time span should be understood in which the subject is able to detect the test signal which, as a matter of fact, usually has near the threshold level.

Obviously enough quite different situation is faced by the listener in case of the automatic audiometers being applied, particularly these equipped with the electronic control of the signal level [9, 11, 12]. In these audiometers the rate of signal level control can be varied in a very wide range. Quite substantial changes in the hearing threshold tracings follow these variations and result in the changes of the hearing threshold level read out from the tracings according to the applied convention pertaining to the averaging of the spikes recorded.

Hence a question appears what rates of the signal level control can be applied and what criteria should be used for the determination of the threshold level from the threshold tracings thus obtained. Particularly it seems to begin questionable if the commonly used method of the linear interpolation can be applied both for low and high rates of the signal control and which phase of the tracing should be regarded as representative for the «true» threshold. The answer to these questions is the attempt of this work. Just to illustrate the divergency in the results of the threshold measurements obtained from automatic audiometry (conventional averaging) and conventional audiometry (the method of limits) which amounts to about 3 dB the report by HEMPSTOCK et al. [7]. can be quoted.

2. The equipment and method

The measurements were made in the sound insulated booth using the Békésy type automatic audiometer with the electronic control of signal level, described in detail in the earlier reports [9, 11, 12]. The last version was used with the threshold equaliser, TDH 39 MX 41—AR headphones and the headphones frequency response equaliser. Continuous sine signal test stimulus of fixed frequency was used in all the measurements (automatic frequency

scanning disconnected) and the discrete frequencies in the successive experiments were 100, 1000 and 8000 Hz. At each of these frequencies the hearing threshold level tracings were made using three rates of the signal level control i.e. 3, 10 and 30 dB/s.

Three music students, two male and one female, aged 24 to 26 otologically normal and with considerable experience in similar experiments served as subjects in the experiments. The measurements were made in individual sessions with each of the subjects who performed in accordance with the known instructions for automatic audiometers [10]. The test signal was delivered to one ear only. Before the actual measurements each listener was obliged to stay in the closed booth for 10 min to reduce the effect of the hearing threshold improvement in silence [3]. The duration of the threshold tracing in all cases was at least 12 min. In this manner several threshold tracings from each listener were obtained each day. Rest periods between the successive tracings were about 30 min. At the beginning of each session listeners had to pass the routine screening test i.e. test threshold tracing at 1 kHz and 3 dB/s. If the mean threshold level traced varied more than ± 1.5 dB the measurements were not continued that day.

The experiment was carried out over the span of three months but the measurements with individual listeners lasting about 1 month were made in succession, so as to collect the individuals data within the possibly short period. The number of tracings from each of the listeners was 10 at 9 points defined by 3 frequency and 3 signal control rates combinations.

3. Data processing and the results of analysis

From each of the hearing threshold tracings thus obtained the fraction from the very beginning up to 60 s was eliminated as pertaining to the initial transient phase [7]. Next, from each 10 s of the tracing over its whole length the mean values L_s and the maximum values L_m of the recorded level were determined, in each case the appropriate method of averaging being applied (i.e. L_s – averaging between the extremes of the record; L_m – averaging between the maximums of the recording).

These data, pertaining to 9 experimental situations (3 frequencies, 3 signal control rates at each frequency) were gathered in assemblages of L_s and L_m containing information referring to the successive 60 s time spans. The assemblages contained 180 L_s and 180 L_m readings (6 readings $\times$ 10 tracings $\times$ 3 listeners = 180). Medians and maximal deviations of L_m and L_s determined from these assemblages are presented in Fig. 1 and Fig. 2.

The overall «by eye» analysis of the $L_s(t)$ and $L_m(t)$ functions reveals quite considerable variability of the hearing threshold level with time and also its dependence on the rate of signal level control. It can be observed at all the three frequencies and all signal control rates used. Therefore it had to be de-

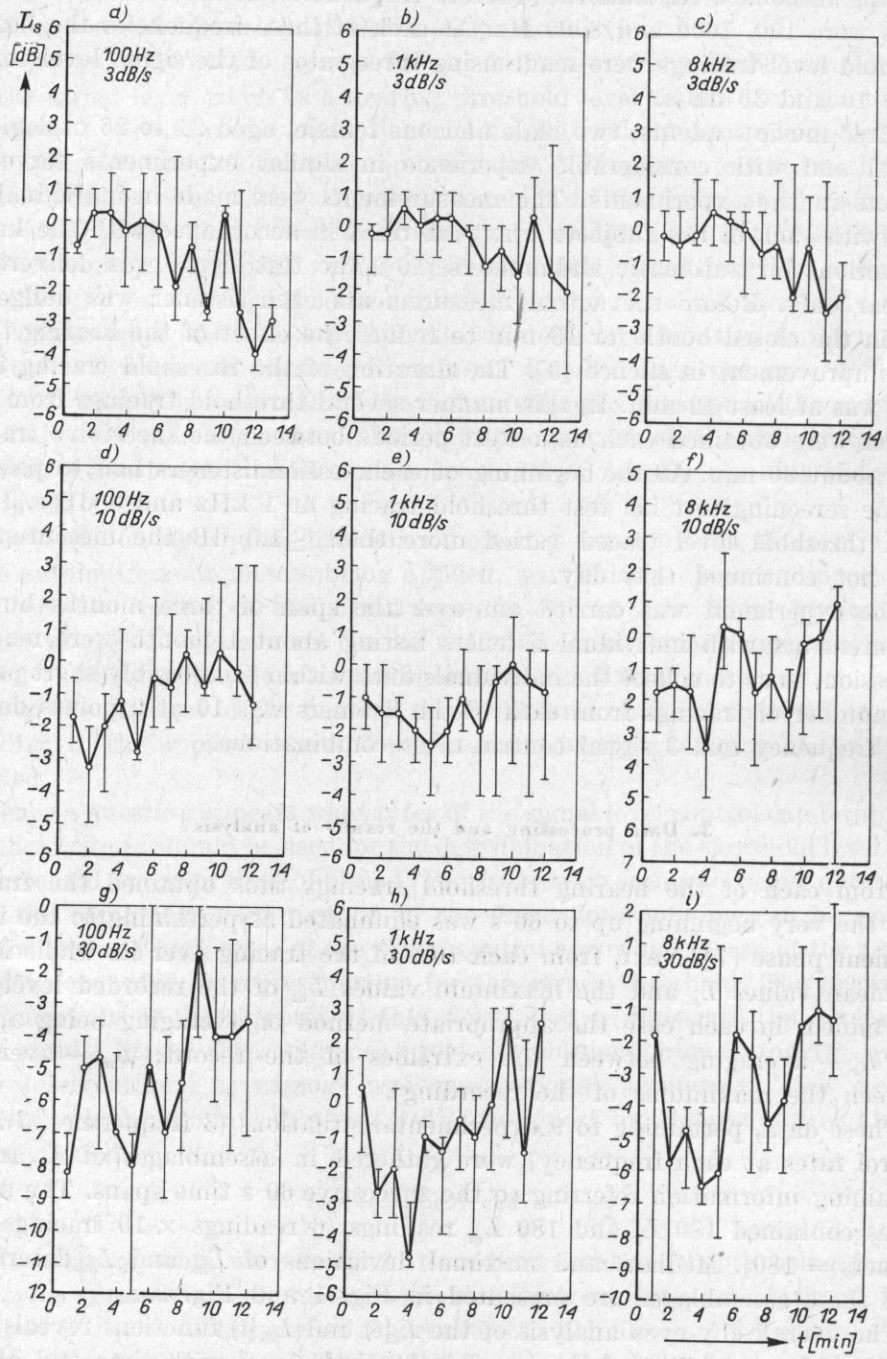

Fig. 1. Medians and dispersion of mean (L_s) hearing threshold levels as a function of time. Frequencies 100, 1000, 8000 Hz; rates of test signal control 3, 10, 30 dB/s

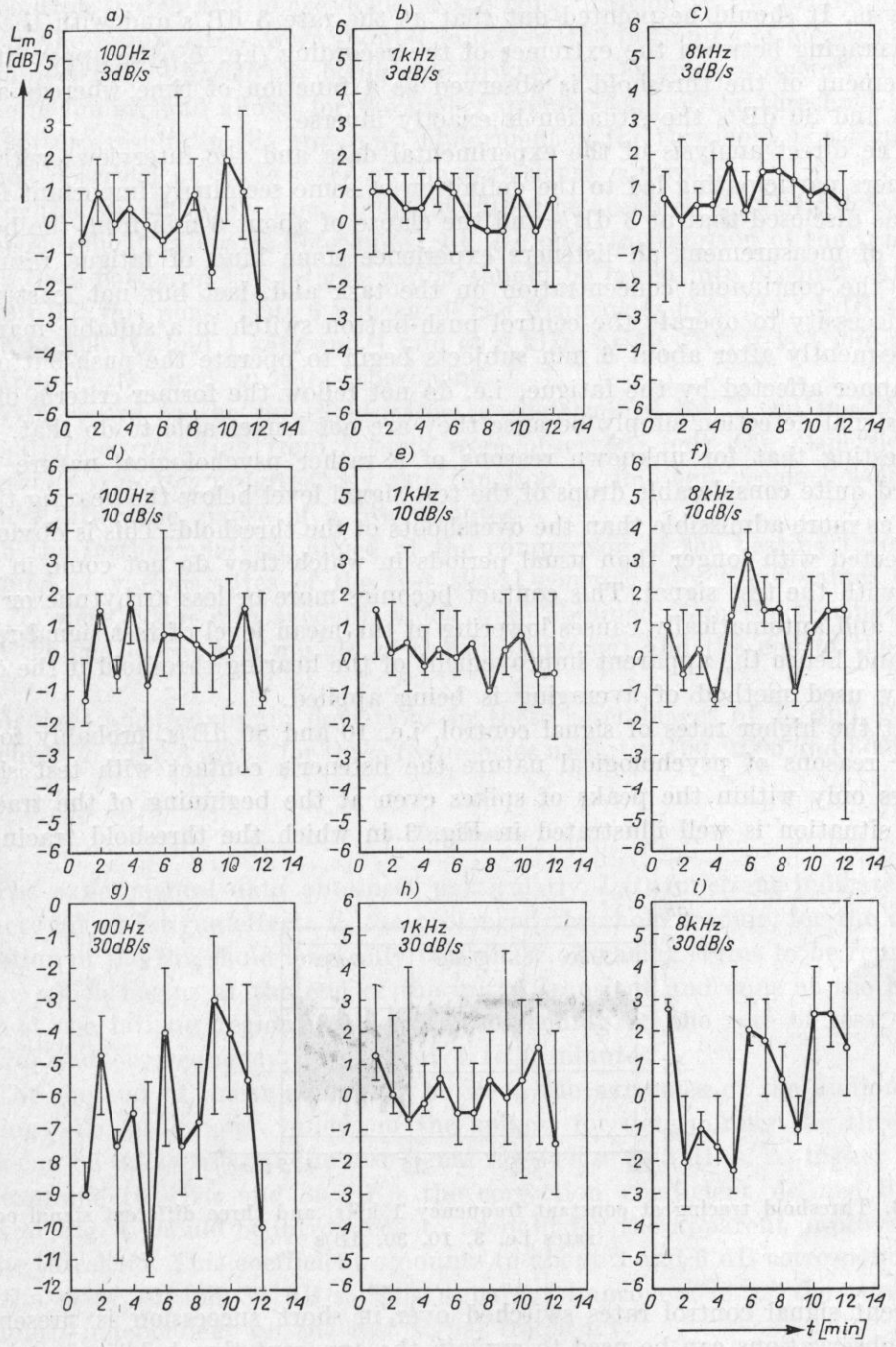

Fig. 2. Medians and dispersion of maximum (L_m) hearing threshold levels as a function of time. Frequencies 100, 1000, 8000 Hz; rates of test signal control 3, 10, 30 dB/s

cided which phase of the obtained functions should be taken for the further analysis. It should be pointed out that at the rate 3 dB/s and with the rule of averaging between the extremes of the recording (i.e. L_s) the apparent improvement of the threshold is observed as a function of time whereas at 10 dB/s and 30 dB/s the situation is exactly inverse.

The direct analysis of the experimental data and the interviews with the listeners participating led to the definition of some seemingly important facts. It was disclosed that at 3 dB/s and the elapse of about 6 min from the beginning of measurement all listeners experience some kind of fatigue resulting from the continuous concentration on the task and, last but not least from the necessity to operate the control push-button switch in a suitable manner. Consequently after about 6 min subjects begin to operate the push-button in a manner affected by the fatigue, i.e. do not follow the former criteria of the test signal detection simply because they are not longer able to do that. It is interesting that for unknown reasons of a rather psychological nature they regard quite considerable drops of the test signal level below the hearing threshold as more admissible than the overshoots of the threshold. This is obviously connected with longer than usual periods in which they do not come in contact with the test signal. This contact becomes more or less arrhytmic or sporadic and automatically causes lowering of the mean level of test signal recorded and hence the apparent improvement of the hearing threshold if the commonly used method of averaging is being applied.

At the higher rates of signal control, i.e. 10 and 30 dB/s, probably for similar reasons of psychological nature the listener's contact with test signal occurs only within the peaks of spikes even at the beginning of the tracing. This situation is well illustrated in Fig. 3 in which the threshold tracing at

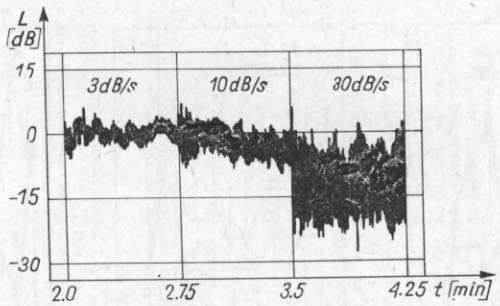

Fig. 3. Threshold tracing at constant frequency 1 kHz and three different signal contro rates i.e. 3, 10, 30, dB/s

different signal control rates switched over in short succession is presented. This observations can be used to explain the apparent threshold improvement as determined by L_s (t) functions at the rates 10 and 30 dB/s over the time span lasting 4 to 6 min. Higher rates of the signal level control (e.g. 10 and

30 dB/s), impose on the subject the necessity of very rapid operation of the push-button switch and hence demand the concentration to the degree higher than at the rate 3 dB/s. After about 4 min from the beginning of measurement the subject finds himself not being able to keep to the rules of operation used at the beginning and allows for the higher overshooting of the threshold level. This in turn results in the apparent impairment of the threshold as a function of time observed at these rates of the test signal control.

For the reasons figured out it should rather be accepted that with reference to the threshold values as determined by L_s, only this portion of the tracings which does not enter the fatigue region should be taken into account. At the rate 3 dB/s this phase lasts 6 min at all the frequencies used. At 10 dB/s it is 6 min at 100 Hz and 1 kHz and 4 min at 8 kHz; at 30 dB/s it is 4 min at all the frequencies used in the experiment.

With regard to the threshold values as determined by L_m no *unidirectional* variations resulting from fatigue were observed; only the dispersion of the results increases progressively as a function of time and becomes well pronounced after the clapse of a few minutes.

In the further analysis, aimed at the comparison of the hearing threshold obtained at various rates of the test signal control, only these values of L_s and L_m were taken into account which were obtained from the tracings between the end of the first minute of the measurement and the end of the fifth minute.

Medians and maximum deviations in these assemblages of L_s and L_m are presented in Figs. 4 and 5 for three frequencies used, i.e. 100, 1000 and 8000 Hz.

4. Discussion

The experimental data obtained, particularly $L_s(t)$ functions indicate that on account of fatigue effects in the prolonged threshold tracing, for the determination of the threshold level only this phase of tracing seems to be representative which begins at the end of the initial transient and ends at the beginning of the fatigue region. This phase, depending on the rate of test signal control and on frequency lasts about 4 to 6 minutes.

The method of linear averaging between the extremes of the audiometric tracings (i.e. peaks and valleys of the spikes) for determining the threshold level can be safely used at the test signal rates close to 3 dB/s. At higher rates, for example 10 dB/s and 30 dB/s the correction coefficient defined by the data in Fig. 4 should be introduced to account for the apparent improvement of the threshold. This coefficient amounts to about 2 and 6 dB correspondingly for the rates 10 and 30 dB/s. This apparent improvement of the threshold is almost independent on the test signal frequency.

The method of linear averaging between the maximums of the tracing (i.e. peaks of the spikes) at the rate 3 dB/s gives about 0.5 to 1.0 improvement

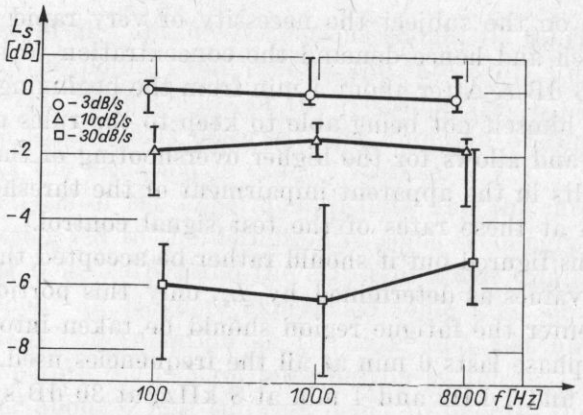

Fig. 4. Medians and deviations of L_s averaged over 4 min of the threshold tracings

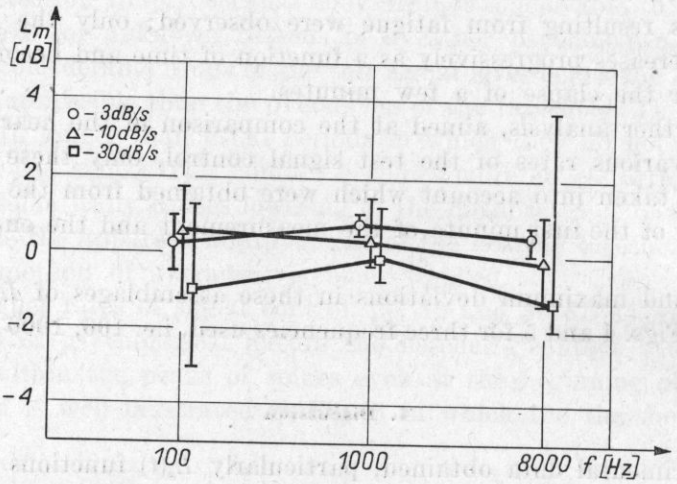

Fig. 5. Medians and deviations of L_m averaged over 4 min of the threshold tracings

of the threshold as compared with the threshold obtained from the linear averaging between the extremes of the tracing. In normal practice this discrepancy is not significant and it can be assumed that at the rate 3 dB/s both methods of reading the tracings are acceptable.

The significant and valuable feature of the method of averaging between the maximums of the tracings is that at higher test signal rates, i.e. 10 and 30 dB/s the threshold is determined directly without the necessity to be corrected by any correction coefficients. As a matter of fact the apparent threshold improvement with this method of interpretation is observed only at 30 dB/s and does not exceede 1 dB. Also, as it is clear from Fig. 2, the threshold thus determined is less dependent on the duration of experiment, at least with regard to the mean value. Only the dispersion obviously increases with time.

It may also be pointed out that the long term variations of L_s at low rates of the test signal control (3 dB/s) and all high rates (10 dB/s and 30 dB/s) go opposite to each other (Fig. 1). This observation suggests that there possibly exists some intermediate rate of signal control at which these variations do not show or are not significant. Inferred from the interpolation of the results obtained at the rates 3 dB/s and 10 dB/s this intermediate rate with possibly lowest time influence on the mean value of the tracing should amount to about 6 dB/s. This conclusion is in agreement, with some experimental data which have not been published so far [11].

References

[1] M. E. BRYAN, H. D. PARBROOK, W. TEMPEST, *A note on quiet threshold shift in the absence of noise*, J. Sound and Vibration, 2, 147 (1965).

[2] M. E. BRYAN, H. D. PARBROOK, W. TEMPEST, *Variation of quiet threshold with low level noise exposure*, Proc. 5th ICA, Liége 1-B-32 (1965).

[3] M. E. BRYAN, W. TEMPEST, *Precision audiometry*, Acta Otolaryngologica, 64 205 (1967).

[4] P. CLOSE, R. G. IRELAND, *Alterations in pure tone threshold following changes in both absolute and differential presure upon the ear*, J. Audiol. Res., 1, 194 (1961).

[5] J. CORSO, *An evaluation of operating conditions on a Békésy – type audiometer*, AMA Arch. Otolaryngol., 61, 649 (1955).

[6] J. CORSO, *Effects of testing methods on hearing thresholds*, AMA Arch. Otolaryngol., 63, 78 (1956).

[7] T. H. HEMPSTOCK, M. E. BRYAN, W. TEMPEST, *Normal operating conditions for free field automatic audiometry*, 5th ICA, Liége, 13-17 (1965).

[8] T. H. HEMPSTOCK, M. E. BRYAN, J. B. C. WEBSTER, *Free field threshold variance*, J. Sound Vib., 4, 33 (1966).

[9] A. JAROSZEWSKI, A. RAKOWSKI, *A Békésy audiometer with electronic signal level control and its application to psychoacoustical measurement*, Archives of Acoustics, **1**, 3 (1976).

[10] A. JAROSZEWSKI, A. RAKOWSKI, *Analysis of the initial fraction of Békésy recording in the threshold audiometry*, Archives of Acoustics, **1**, 4 (1976).

[11] T. ŁĘTOWSKI, *Personal communication* [based on unpublished data (1976)].

[12] A. RAKOWSKI, A. JAROSZEWSKI, T. ŁĘTOWSKI, *Békésy's audiometer with standard Brüel and Kjaer laboratory equipment* [in Polish], Arch. Akustyki, **4**, 3, 247 (1969).

[13] A. RAKOWSKI, A. JAROSZEWSKI, T. ŁĘTOWSKI, *Automatic audiometer*, Pat. PRL No 138238 (1975).

[14] B. M. SIEGENTHALER, *Reaction time, difference limen and amplitude of excursion of normal Békésy audiogram*, J. Auditory Res., 1, 285 (1961).

[15] J. ZWISLOCKI, F. MAIRE, A. S. FELDMAN, H. RUBIN, *On the effect of practice and motivation on the threshold of audibility*, Jour. Acoust. Soc. Am., **30**, 254 (1958).

Received on 10th July 1976